atoms

MDPI

Article

Electron-Impact Excitation and Dissociation of Heavy Rare Gas Heteronuclear Ions via Transitions to Charge Transfer States

Alexander Narits *, Konstantin Kislov and Vladimir Lebedev

P. N. Lebedev Physical Institute of Russian Academy of Sciences, 119991 Moscow, Russia
* Correspondence: narits@lebedev.ru

Abstract: Heteronuclear diatomic rare gas molecular cations feature excited electronic terms with charge transfer character located several eV above the ground term. The role of such terms in collisions involving heteronuclear ions is studied theoretically under conditions typical of the plasma-based sources of UV and IR radiation. Calculations were carried out for processes of dissociative excitation, dissociative recombination and electron impact bound–bound excitation in Ar/Xe and Kr/Xe plasmas using the recently developed semiclassical approach combined with the *ab initio* data for potential energy curves and oscillator strengths of electronic transitions. The approach consistently describes the contributions from the entire rovibrational manifold to the processes studied. The cross sections of the processes mentioned are calculated for wide ranges of gas temperatures and electron energies. We show that the processes considered are quite effective when they are accompanied by transitions to charge transfer terms. For the range of electron energies typical of active media of UV and IR radiation sources the cross sections exceed those reported for the processes usually considered to involve transitions between the ground and first excited electronic state. The excitation of charge transfer electronic terms can play an important role in the kinetics of rare gas mixture plasmas.

Keywords: noble gases; heteronuclear ions; dissociation and excitation; charge transfer; electron impact

PACS: 34.50.Gb; 34.70.+e; 34.80.Ht; 34.80.Lx

Citation: Narits , A.; Kislov, K.; Lebedev, V. Electron-Impact Excitation and Dissociation of Heavy Rare Gas Heteronuclear Ions via Transitions to Charge Transfer States. *Atoms* **2023**, *11*, 60. https://doi.org/10.3390/atoms11030060

Academic Editor: Ioan Schneider

Received: 31 January 2023
Revised: 7 March 2023
Accepted: 15 March 2023
Published: 17 March 2023

1. Introduction

Plasmas of rare gas mixtures are among the most commonly used types of active media for VUV excimer lamps [1–3], microplasma arrays [4,5], optically pumped rare gas lasers (OPRGLs) [6,7] and powerful IR lasers [8]. The principal advantage of using rare gases in the active media of various electromagnetic radiation sources consists in their having relatively low chemical activity, which reduces non-radiative losses and simplifies the development of schemes of the population of the upper levels of working transitions [9]. As compared to the plasmas formed in the medium of a single noble gas element, binary mixtures, like Ar/Xe, Ne/Xe, Kr/Xe, Ar/Kr, etc., allow for a more efficient population of the required excited atomic states of the heavier element of the mixture, via a variety of collisional processes (see [10] and references therein).

The binary mixture B/A plasmas feature a number of atomic, A, A^+, A^*, B, B^+, B^*, and molecular, A_2, A_2^+, B_2, B_2^+, BA, BA^+, constituents. Usually, the concentrations of the main, heavier element, A, is much smaller than the concentration of the buffer gas, B. Owing to the variety of possible reaction partners, the theoretical description of the operation of the radiation sources, based on rare gas mixture plasmas, requires the development of quite sophisticated kinetic models [1,3,11,12], which take into account the collisional and radiative processes involved with most of these species. Heteronuclear noble gas ions BA^+ containing at least one heavy rare gas element are characterized by small dissociation energies, D_0 = 13.1, 33, 179, and 389 meV [13] for $HeXe^+$, $NeXe^+$, $ArXe^+$, and $KrXe^+$, respectively, and strong spin–orbit interaction (of the order of a few electron-volts), and are

best described in terms of Hund's "c" type of angular momenta coupling. Such properties complicate the experimental and theoretical studies of these ions [14], so that the available data on the processes which occur with the participation of the heavy heteronuclear noble gas cations are rather sparse, in comparison to the homonuclear species. Most modern kinetic models of plasmas of binary or ternary rare gas mixtures rely on the approximate formula [15] for the rate constant of the dissociative recombination of such heteronuclear ions. Experimental studies of the emission spectra of heavy rare gas $ArXe^+$ and $KrXe^+$ ions were carried out in [16–19]. The processes of dissociative recombination, resonant ternary electron capture to Rydberg states and dissociative excitation of $RgXe^+$, Rg = He, Ne, Ar, Kr ions, which occur via non-adiabatic transitions between the ground and first excited electronic terms of the ions, were studied in a series of works [20–22].

The heteronuclear molecular cations BA^+, in addition to the electronic terms which dissociate to the combinations of various states of atom B and ion A^+, also feature the electronic terms with charge transfer character, which dissociate to combinations of states of atom A and ion B^+. For heavy heteronuclear rare gas cations the lowermost charge transfer states are denoted as $|B\,1/2\rangle$, $|C\,1/2\rangle$ and $|C\,3/2\rangle$ (1/2 and 3/2 are the magnitudes of the projection Ω of the total electronic angular momentum onto the nuclear axis in Hund's "c" type of coupling), and are separated from the ground electronic term by 2–12 eV (see [23] and references therein). The role of these states in the radiative properties of rare gas mixture plasmas have been studied in, for example, [17,18,24]. The influence of the transitions to charge transfer (CT) states of heteronuclear ions of astrophysical importance (primarily, HeH^+) on the dynamics of dissociative recombination and dissociative excitation was considered in, for example, [25–27]. In contrast to that, the contribution of the CT terms to the dynamics of collisional processes in rare gas mixture plasmas, have not yet, to the best of our knowledge, been considered in the literature. However, at least for $ArXe^+$ and $KrXe^+$ ions, the energy separation of CT terms from the ground electronic state, equal to ≈3.5–4 eV and ≈2–2.8 eV [13,14,24], respectively, is within the typical range of mean electron energies, 1–10 eV [11,28,29], of the rare gas mixture plasmas used as active media of the UV and IR range radiation sources mentioned above. Given that $|B\,1/2\rangle$ and $|C\,1/2\rangle$ states allow for dipole transitions from the ground state, $|X\,1/2\rangle$, one can expect that the collisional processes involving the CT states of heavy noble gas heteronuclear cations could play an important role in the kinetics of rare gas mixture plasmas.

In this work, the results of theoretical studies of the resonant processes which occur during the collisions of $RgXe^+$ ions (Rg = Ar, Kr) with electrons, accompanied by non-adiabatic transitions of the cations to states with charge transfer character, are reported. We consider the following reaction channels: (i) dissociative excitation (DE) of the molecular ions, via transitions to CT states; (ii) the bound–bound transitions of $RgXe^+$ ions, induced by electron impact; and (iii) dissociative recombination (DR) of $RgXe^+$ ions with electrons, via transitions to CT states. For each of the processes, the Boltzmann-averaged cross sections were calculated in the range of gas temperatures and incident electron energies typical of Rg/Xe mixture plasmas used as active media of powerful UV and IR radiation sources. We show that the reactions above can be quite efficient in the range of the plasma parameters considered, with magnitudes of the cross sections similar to those of DE and DR processes accompanied by the transition to first excited term of $RgXe^+$ considered before [21,22].

The theoretical treatment is based on the original approach [20,22,24,30] developed for the description of the radiative and collisional non-adiabatic transitions in homonuclear and heteronuclear cations. It allows one to account for the contributions of the entire rovibrational quasicontinuum to the cross sections and rate constants of the processes studied, which is essential when dealing with weakly and moderately bound ions at room and elevated temperatures. Here we note that high-precision calculations of the processes resulting from the collisions of low-energy electrons with molecular cations can be carried out on the basis of the multi-channel quantum defect theory (MQDT) [31], usually with the help of the *R*-matrix method [32]. Such an approach provides a self-consistent description of disso-

ciative recombination, dissociative excitation and vibrational excitation processes and was successfully used in the studies of reactive electron collisions with various heteronuclear molecular cations of astrophysical importance (see, for example, recent works [33–36]). Reliable results can also be obtained with the help of the molecular convergent close-coupling method [37], as was demonstrated for HeH^+ in [27]. These methods, while providing highly-accurate data for the cross sections of the processes considered, require enormous computational effort when one has to deal with molecular systems under conditions of strong thermal excitation of rotational and vibrational degrees of freedom of the cations, owing to a huge number of states contributing to the processes. For the ions considered in this paper, $ArXe^+$ and $KrXe^+$, the dissociation energies and first vibrational quanta are small enough to ensure the population of the entire rovibrational manifold even at room temperatures. At the same time, for the system under the physical conditions described, one is rarely interested in the cross sections of the processes above originating from a single rotational–vibrational state. Statistically-averaged cross sections or rate constants have more relevance to the experimentally measurable quantities. The theoretical method used in the present work was specifically developed for the description of the integral cross sections of DR, DE and electron-impact excitation processes, taking into account the contributions from all rovibrational states. Despite employing a simplified picture of the dynamics of the processes treated, it was previously shown in [20,22,24,30] to provide results in good agreement with experimental data.

The paper is organized as follows: the processes considered and the specifics of their dynamics are discussed in Section 2. A brief description of the theoretical approach and the formulae used in the calculations is given in Section 3. The results obtained are presented in Section 4. The results are further discussed and some concluding remarks are made in Section 5.

2. Formulation of the Problem

Three competing reactions, which occur in the collisions of $BA^+ \equiv RgXe^+$ (Rg = Ar, Kr) ions with electrons, are considered:

$$BA^+(i, vJ) + e \rightarrow AB^+(f, E') + e \rightarrow A + B^+ + e, \quad (1)$$

$$BA^+(i, vJ) + e \rightarrow AB^+(f, v'J') + e, \quad (2)$$

$$BA^+(i, vJ) + e \rightarrow AB(f, E', nl) \rightarrow B(nl) + A, \quad (3)$$

where i and f denote the initial and final electronic terms of BA^+ ion, vJ is the rovibrational state of the ion before the collision, $E' > 0$ is the energy of the internuclear motion in the final term if the nuclei are not bound after the transition, $v'J'$ is the rovibrational state of the bound BA^+ ion in the final electronic term, and nl denote the principal and angular quantum number of the Rydberg state to which the incident electron can be captured during the collision. Process (1) is the dissociative excitation of BA^+ molecular ion by electron impact, which is accompanied by the transition of the ion to the excited term with charge transfer character, and, in the case of $RgXe^+$ ions, results in the formation of Xe atom in the ground state, and the positive ion of either argon or krypton. Alternatively, when the incident electron does not deposit enough of its energy to $RgXe^+$ ion, an electron-impact bound–bound excitation (2) may occur, which promotes the $RgXe^+$ ion to some $v'J'$ bound state in one of the states with charge transfer character. The incident electron may also get captured into a Rydberg nl-state of Ar or Kr via dissociative recombination process (3) realized via transitions to CT states and subsequent dissociation of the AB^* quasimolecule. As the ground state of $RgXe^+$ is $|X\,1/2\rangle$, the reactions dominantly proceed by dipole-allowed transitions to $|B\,1/2\rangle$ and $|C\,1/2\rangle$ states, while the contribution of dipole-forbidden transitions to $|C\,3/2\rangle$ is negligible.

All three processes (1)–(3) can be described as non-adiabatic transitions in the $BA^+ + e$ system, which occur in the vicinity of the crossing of the potential energy curves of the ground, $U_i(R) + \varepsilon$, and excited, $U_f(R) + \varepsilon'$, electronic terms, with the latter having a charge transfer character. Here $U_i(R)$ and $U_f(R)$ are the potential energy curves of BA^+ ion in the initial, $|i\rangle$, and final, $|f\rangle$, states, while ε and ε' are the energies of the incident electron before and after the collision. The magnitude of ε' can be either positive, which corresponds to the free motion of the electron in the final channel of reactions (1) and (2), or negative, which corresponds to the electron capture into a bound Rydberg state (with the energy of $\varepsilon' = -Ry/n_*^2$) in reaction (3). The position of the crossing, R_ω, is given by the Frank–Condon principle,

$$\Delta U_{fi}(R_\omega) = U_f(R_\omega) - U_i(R_\omega) = \varepsilon - \varepsilon'. \quad (4)$$

For given ε and ε', this condition allows one to determine the values of the internuclear distance R, at which the incident electron may resonantly exchange energy with the electronic subsystem of the molecular cation (see Figure 1).

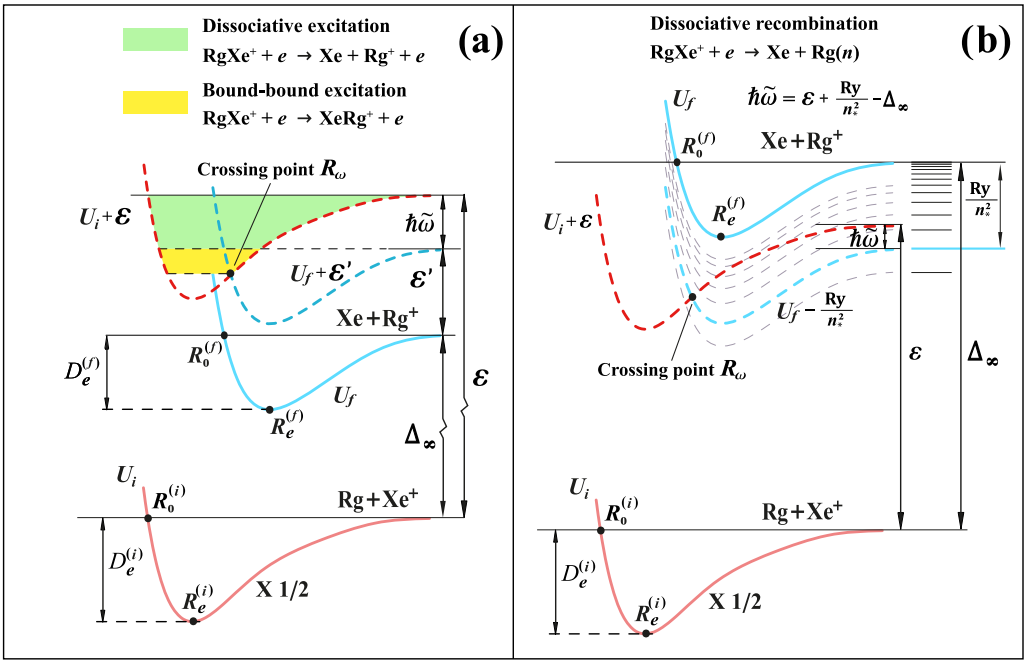

Figure 1. Schematics of the non-adiabatic transitions in $RgXe^+ + e$ system responsible for processes considered in the present work. (**a**) Dissociative excitation and electron-impact bound–bound excitation to charge transfer terms. (**b**) Dissociative recombination via transitions to charge transfer terms. Solid red and light-blue lines denote the initial, $U_i(R)$, and final, $U_f(R)$, electronic terms of $(RgXe)^+$ ion. Dashed red and blue lines denote the effective electronic terms, $U_i(R) + \varepsilon$ and $U_f(R) + \varepsilon'$, of the $RgXe^+ + e$ system in the initial and final states, respectively. Gray dashed lines depict the effective molecular Rydberg states, $U_f(R) - Ry/n_*^2$, of the Rg^*Xe molecule converging to a CT-type excited term of $RgXe^+$ ion.

3. Brief Description of the Theoretical Approach

The theoretical treatment is based on an approach [20,22,30] initially developed for the description of radiative and collisional transitions between the attractive ground state term and repulsive excited term of diatomic molecular cations. The approach combines the *Rice*-type of the theory of non-adiabatic transitions [38] with the analytic technique [39] for the summation over all rovibrational states of the BA^+ ion. It allows one to provide a self-consistent description for the contribution from the entire manifold of rovibrational states, as well as from the continuum to the cross sections and rate constants of the processes considered. The approach was recently generalized [24] to the case of the attractive upper

state, which made it applicable to the investigation of the non-adiabatic processes involving transitions to the charge transfer terms of $RgXe^+$ (Rg = Ar, Kr) ions discussed herein.

3.1. Cross Sections of the Dissociative Excitation and Electron-Impact Bound–Bound Excitation Involving Transitions to Charge Transfer Terms

We studied the dynamics of processes (1)–(3) at gas temperatures typical of the active media of plasma-based sources of UV and IR radiation, T=300–900 K. Owing to the relatively small dissociation energies of $ArXe^+$ and $KrXe^+$ cations, such temperatures resulted in the strong excitation of the entire rovibrational quasicontinuum of the ions in the initial channel of the reactions considered. As the number of the individual vJ states contributing to the reactions is huge, one is mainly interested in the Boltzmann-averaged cross sections of the processes studied. Within our approach the channels of the dissociative excitation (1) and bound–bound transitions induced by electron impact (2) were treated in the unified manner and only differed in the ranges of the rovibrational states that were energetically allowed to participate in the specific processes,

$$\sigma_T^{(\mathrm{ch})}(\varepsilon) = \sum_{vJ\in(\mathrm{ch})} \sigma_{vJ}^{(\mathrm{ch})}(\varepsilon)\left(N_{\mathrm{BA}^+(i,vJ)}/N^{\mathrm{tot}}_{\mathrm{BA}^+(i)}\right), \quad N^{\mathrm{tot}}_{\mathrm{BA}^+(i)} = \sum_{vJ} N_{\mathrm{BA}^+(i,vJ)}, \quad (\mathrm{ch}) = \{\mathrm{de}, \mathrm{cte}\}. \tag{5}$$

Here indices "de" and "cte" denote the processes (1) and (2), correspondingly; $\sigma_{vJ}^{(\mathrm{ch})}(\varepsilon)$ [cm^2] are the cross sections of each of the processes (ch) = {de, cte} calculated for $BA^+ \equiv RgXe^+$ ion populating vJ in the initial channel. The summation was carried out over the range $vJ \in (\mathrm{ch})$ of vJ-states which are permitted by the energy conservation law applied to process (ch). The quantity $N_{\mathrm{BA}^+(i,vJ)}$ denotes the concentration of molecular ions in specific vJ state, whereas $N^{\mathrm{tot}}_{\mathrm{BA}^+(i)}$ is the total concentrations of BA^+ ions in bound states of the initial term. For the Boltzmann distribution over the rovibrational states Equation (5) becomes

$$\sigma_T^{(\mathrm{ch})}(\varepsilon) = \frac{1}{\mathfrak{s} Z_{\mathrm{vr}}(T)} \sum_{vJ\in(\mathrm{ch})} (2J+1)\sigma_{vJ}^{(\mathrm{ch})}(\varepsilon)\exp\left(-\mathcal{E}_{vJ}/k_{\mathrm{B}}T\right), \tag{6}$$

where

$$Z_{\mathrm{vr}}(T) = \frac{1}{\mathfrak{s}}\sum_{vJ}(2J+1)\exp\left(-\mathcal{E}_{vJ}/k_{\mathrm{B}}T\right) \tag{7}$$

is the rovibrational partition function of $BA^+(i)$ in the initial term, and $\mathfrak{s}$ is a symmetry factor equal to 1 or 2 for the heteronuclear and homonuclear diatomic molecular cations, respectively. The rovibrational energy, $\mathcal{E}_{vJ}$, is taken relative to the bottom of the potential well of $U_i(R)$. The huge number of participating vJ states make it possible to use the quasicontinuous spectrum approximation for vJ and $v'J'$ levels. As follows from [24,40], in this approximation the formulae for the cross sections $\sigma_{vJ}^{(\mathrm{ch})}(\varepsilon)$ of the processes of dissociative excitation (1) and electron-impact bound–bound excitation (2) from a given vJ state are identical. Therefore, the resulting expressions for the averaged cross sections $\sigma_T^{(\mathrm{ch})}(\varepsilon)$, (ch) = {de, cte} only differ in the area of integration over the quasicontinuum of rovibrational states. After the integration, Equation (6) can be written as

$$\sigma_T^{(\mathrm{ch})}(\varepsilon) = \frac{g_{\mathrm{BA}^+(f)}}{g_{\mathrm{BA}^+(i)}\mathfrak{s}}\frac{8\pi^3}{k^2 Z_{\mathrm{vr}}(T)}\left(\frac{\mu k_{\mathrm{B}}T}{2\pi\hbar^2}\right)^{3/2}\exp\left(-\frac{D_0^{(i)}}{k_{\mathrm{B}}T}\right)\int\limits_{R_{\min}(\varepsilon)}^{\infty}\Gamma_{\varepsilon\to\varepsilon'}(R_\omega)\exp\left(-\frac{U_i(R_\omega)}{k_{\mathrm{B}}T}\right)\Theta_T^{(\mathrm{ch})}(R_\omega)R_\omega^2 dR_\omega, \tag{8}$$

Here $g_{\mathrm{BA}^+(i)}$ and $g_{\mathrm{BA}^+(f)}$ are the statistical weights of the initial and final electronic terms of the ion, and $D_0^{(i)}$ is the dissociation energy of BA^+ in the initial state. The lower integration limit, $R_{\min}(\varepsilon)$, is determined by the condition of $\Delta U_{fi}(R_{\min}(\varepsilon)) = \varepsilon \equiv \hbar^2k^2/2m_e$,

where k is the wavenumber of the incident electron and m_e is the electron mass. Dimensionless quantity $\Gamma_{\varepsilon\to\varepsilon'}(R_\omega)$ is the effective coupling parameter,

$$\Gamma_{\varepsilon\to\varepsilon'}(R) = \sum_{lm,l'm'} \Gamma_{\varepsilon' l' m',\varepsilon lm}(R) \longrightarrow 2\pi \sum_{lm,l'm'} \left| \mathrm{V}^{f,\varepsilon' l' m'}_{i,\varepsilon lm}(R) \right|^2, \tag{9}$$

which can be expressed through the matrix element of electronic transition

$$\mathrm{V}^{f,\varepsilon' l' m'}_{i,\varepsilon lm}(\mathbf{R}) = \left\langle \psi_{\varepsilon' l' m'}(\mathbf{r}) \middle| \left\langle \varphi_f(\mathbf{r}_k,\mathbf{R}) | \mathrm{V} | \varphi_i(\mathbf{r}_k,\mathbf{R}) \right\rangle \middle| \psi_{\varepsilon lm}(\mathbf{r}) \right\rangle. \tag{10}$$

Here $\psi_{\varepsilon lm}(\mathbf{r})$ and $\psi_{\varepsilon' l' m'}(\mathbf{r})$ are the wavefunctions of the outer electron of $\mathrm{BA}^+ + e$ system before and after the collision, whereas wavefunctions $\varphi_i(\mathbf{r}_k,\mathbf{R})$ and $\varphi_f(\mathbf{r}_k,\mathbf{R})$ describe the electronic shell of BA^+ ion in the initial, $U_i(R)$, and final, $U_f(R)$, electronic terms. The perturbation V denotes the interaction between the incident electron and all inner electrons of the molecular cation.

The dimensionless factor $\Theta_T^{(\mathrm{ch})}(R_\omega)$, (ch) = de, cte, in (8) describes the relative roles of the competing processes of dissociative excitation (1) and electron-impact bound–bound excitation of molecular ions (2). Within semiclassical approximation, the expressions for $\Theta_T^{\mathrm{de}}(R_\omega)$ and $\Theta_T^{\mathrm{cte}}(R_\omega)$ coincide with the formulae obtained in [40] for the processes of photodissociation of bound–bound phototransitions of diatomic cations, respectively

$$\Theta_T^{\mathrm{de}}(R_\omega) = \begin{cases} 0, & R_\omega < R_0^{(i)}, \\ \dfrac{\gamma(3/2,|U_i(R_\omega)|/k_\mathrm{B}T)}{\Gamma(3/2)}, & R_0^{(i)} \le R_\omega \le R_0^{(f)}, \\ \dfrac{\gamma(3/2,|U_i(R_\omega)|/k_\mathrm{B}T)}{\Gamma(3/2)} - \dfrac{\gamma(3/2,|\widetilde{U}_f(R_\omega)|/k_\mathrm{B}T)}{\Gamma(3/2)}, & R_x > R_\omega \ge R_0^{(f)}, \\ 0, & R_\omega \ge R_x. \end{cases} \tag{11}$$

$$\Theta_T^{\mathrm{cte}}(R_\omega) = \begin{cases} 0, & R_\omega < R_0^{(f)}, \\ \dfrac{\gamma(3/2,|\widetilde{U}_f(R_\omega)|/k_\mathrm{B}T)}{\Gamma(3/2)}, & R_x \ge R_\omega \ge R_0^{(f)}, \\ \dfrac{\gamma(3/2,|U_i(R_\omega)|/k_\mathrm{B}T)}{\Gamma(3/2)}, & R_\omega \ge R_x. \end{cases} \tag{12}$$

Here, we introduced the effective upper electronic term $\widetilde{U}_f(R_\omega) \equiv U_f(R_\omega) - \Delta U_{fi}(R \to \infty)$ in such a way that the terms of $U_i(R_\omega)$ and $\widetilde{U}_f(R_\omega)$ have the same energy in the dissociation limit. Values $R_0^{(i)}$ and $R_0^{(f)}$ of the internuclear distance are determined from conditions $U_i(R_0^{(i)}) = 0$ and $\widetilde{U}_f(R_0^{(f)}) = 0$, respectively. The distance R_x corresponds to the intersection of the curves U_i and $\widetilde{U}_f$, $U_i(R_x) = \widetilde{U}_f(R_x)$ (which is equivalent to $\Delta U_{fi}(R_x) = \Delta U_{fi}(R \to \infty)$). Functions $\Gamma(x)$ and $\gamma(x,y)$ are the Euler gamma, and lower incomplete Euler gamma functions, respectively.

It can be seen from (11) and (12) that the expression for the sum of the relative contributions, $\Theta_T^{\mathrm{de}}(R_\omega) + \Theta_T^{\mathrm{de}}(R_\omega)$, coincides with the expression for dimensionless factor $\Theta_T(R_\omega)$ for the non-adiabatic dissociation processes (dissociative recombination, dissociative excitation and photodissociation) when the upper term $U_f(R)$ is purely repulsive.

3.2. Cross Sections of Dissociative Recombination of BA^+ *Ions via Transitions to Charge Transfer Terms*

The process of the dissociative recombination of BA^+ with electrons, which occurs via non-adiabatic transitions to the electronic terms with charge transfer character, and leads to electron capture to the atomic Rydberg states B(nl), is described using the approach developed in our previous work [20,21]. The approach treated the dissociative recombination process in heteronuclear rare gas ions accompanied by the transitions to the first

excited electronic state which has a repulsive potential energy curve. Similar to the process of dissociative excitation, the theoretical model of the DR process is based on the theory of non-adiabatic transitions and the quasicontinuous approximation for the rovibrational states of the molecular cation. In order to study the dissociative recombination involving electronic states with charge transfer character, we have generalized the approach to account for the presence of the potential well in the upper term. It is important to note that here we only consider the direct mechanism of DR (see, for example, [41]), realized via non-adiabatic transitions at the crossings of the effective potential energy curves of $BA^+ + e$ system. Such an approach is unable to reproduce the well-known low-energy resonances in the cross sections of a dissociative recombination process [41] originating from individual vibrational states, which can be described using more sophisticated methods, based on MQDT [33–36,41] or the Complex Kohn Variation method [41]. These methods, while yielding undoubtedly more precise results, are quite problematic to apply in situations when the rovibrational states of the systems studied are strongly excited, as the number of participating states becomes huge. Under such conditions, the resonances mentioned above get smeared out [42,43], and the simplified treatment of the Boltzmann-averaged cross sections of DR used herein produces results in good agreement with more sophisticated approaches, as was demonstrated in [20].

Following the procedure outlined in [21,24], the expression for the Boltzmann-averaged cross section of the process (3) was obtained,

$$\sigma_{nl}^{\mathrm{dr}}(\varepsilon,T)=\frac{g_{\mathrm{BA}^+(f)}}{g_{\mathrm{BA}^+(i)}\mathfrak{s}}\frac{8\pi^3(2l+1)R_\omega^2}{k^2Z_{\mathrm{vr}}}\frac{\Gamma_{nl\to\varepsilon}(R_\omega)}{\Delta F_{fi}(R_\omega)}\left(\frac{\mu k_{\mathrm{B}}T}{2\pi\hbar^2}\right)^{3/2}\exp\left(-\frac{D_0^{(i)}+U_i(R_\omega)}{k_{\mathrm{B}}T}\right)\Theta_T^{\mathrm{dr}}(R_\omega). \tag{13}$$

Here $\Delta F_{fi}(R_\omega)=\left|F_f(R_\omega)-F_i(R_\omega)\right|$ is the difference between the slopes, $F_i=-\frac{dU_i}{dR}\Big|_{R_\omega}$ and $F_f=-\frac{dU_f}{dR}\Big|_{R_\omega}$, of the initial, U_i, and final, U_f, electronic terms calculated at point R_ω given by

$$U_i(R_\omega)+\frac{\hbar^2k^2}{2m_e}=U_f(R_\omega)-\frac{Ry}{n_*^2}. \tag{14}$$

The binding energy of the Rydberg electron in B(nl) state is expressed in (14) as $\frac{Ry}{n_*^2}\equiv|\varepsilon_{nl}|$ (see Figure 1). We note here that our approach for the description of the dynamics of DR process used the approximation of atomic quantum defects for Rydberg states of the B*A quasimolecule. In a general case, the quantum defects $\delta_{nl}=n-n_*$ of the excited molecular states are R-dependent, and should either be obtained from an analysis of the spectroscopic data, or determined by the high-level ab initio calculations of the potential energy curves of the Rydberg states and the respective ionic states. To our knowledge, no data for the R-dependent quantum defects of Rg(nl)Xe, Rg = Ar, Kr, with $n\approx10$ are currently available. However, the simplified model for the treatment of the Rydberg states of heteronuclear rare gas dimers [44], which was able to give a reasonable description of the experimental data on photoionization of ArKr, ArXe and KrXe [45], suggested that it is permissive to treat the molecular Rg*Xe states as perturbed atomic states Rg*. This justifies the use of the atomic quantum defects in the present work.

The quantity of $\Gamma_{nl\to\varepsilon}(R)$ in (13) is the autoionization width of the quasimolecular Rydberg state AB(nl). It can be expressed through the matrix element of the interaction of the incident electron with the nuclei and all electrons of the molecular cation as follows:

$$\Gamma_{nl\to\varepsilon}(R)=\frac{2\pi}{2l+1}\sum_{m,m'l'}\left|\mathrm{V}_{i,\varepsilon l'm'}^{f,nlm}(R)\right|^2,$$
$$\mathrm{V}_{i,\varepsilon l'm'}^{f,nlm}(\mathbf{R})=\langle\psi_{\varepsilon l'm'}(\mathbf{r})|\langle\varphi_i(\mathbf{r}_\kappa,\mathbf{R})|\mathrm{V}(\mathbf{r}_\kappa,\mathbf{R})\Big|\varphi_f(\mathbf{r}_k,\mathbf{R})\Big\rangle|\psi_{nlm}(\mathbf{r})\rangle \tag{15}$$

The factor $\Theta_T^{\mathrm{dr}}(R_\omega)$ in Equation (13) describes the integral contribution of the bound states of the internuclear motion to the total cross section of the electron capture in the

$BA^+ + e$ system. The formula for $\Theta_T^{\rm dr}(R_\omega)$ is identical to that of the relative efficiency of the dissociative excitation process (11), $\Theta_T^{\rm dr}(R_\omega) = \Theta_T^{\rm de}(R_\omega)$.

Total cross sections of the dissociative recombination (3) resulting in the population of Rydberg $B(n)$ levels are obtained via summing of (13) over all nl-sublevels with a given value of n.

3.3. Evaluation of the Coupling Parameter and the Autoionization Width

When a non-adiabatic transition occurs between two terms for which the radiative electric dipole transitions are allowed, one can usually expand the interaction of the incident electron with the electrons of the molecular cation into the multipole expansion and truncate the series at the dipole term [46]. Then, for the dipole-allowed $X\,1/2 \to B\,1/2$ and $X\,1/2 \to C\,1/2$ transitions considered herein, it is possible to use the dipole approximation for the perturbation. As a result, the coupling parameter (see Section 3.1) and the autoionization width (see Section 3.2) can be expressed via the dipole transition electronic matrix element. For $\Gamma_{\varepsilon\to\varepsilon'}(R)$ this yields (see [47] and references therein)

$$\Gamma_{\varepsilon\to\varepsilon'}(R_\omega) = \frac{4\,G_{\varepsilon\to\varepsilon'}}{3\sqrt{3}}\left|\frac{d_{fi}(R_\omega)}{ea_0}\right|^2, \tag{16}$$

where a_0 is the Bohr radius, $d_{fi}(R_\omega)$ is the dipole matrix element of transition between terms U_i and U_f, and $G_{\varepsilon\to\varepsilon'}$ is the Gaunt factor [46] equal to 1 in the semiclassical Kramers approximation. Similarly, $\Gamma_{nl\to\varepsilon}(R_\omega)$ can be evaluated using the semiclassical formula for the matrix element of the electron coordinate between the wavefunctions of discrete and continuous spectra,

$$\Gamma_{nl\to\varepsilon}(R_\omega) = \frac{\hbar\omega(l+1/2)^4}{3\pi n_*^3}\mathrm{f}_{fi}(R_\omega)\left[K_{2/3}^2(u) + K_{1/3}^2(u)\right], \quad \mathrm{f}_{fi}(R_\omega) = \frac{2m_e\omega\left|d_{fi}(R_\omega)\right|^2}{3\hbar e^2}, \tag{17}$$

where $K_\nu(u)$ is the McDonald function, $u = \hbar\omega(l+1/2)^3/6\mathrm{Ry}$, $\hbar\omega = \varepsilon + |\varepsilon_{nl}| \equiv \hbar\tilde{\omega} + \Delta_\infty$, $\Delta_\infty \equiv \Delta U_{fi}(R\to\infty)$, and $\mathrm{f}_{fi}(R_\omega)$ is the oscillator strength of the electronic transition in BA^+ ion.

As follows from (4) and (17), the calculations of the resonant transition points R_ω and autoionization widths $\Gamma_{nl\to\varepsilon}(R_\omega)$ require the data on the effective principal quantum number of Rydberg levels of Ar and Kr. It should be noted that Rydberg states $\mathrm{Rg}[5p^5(^2P_j)nl[K]_{\mathcal{J}}]$ (Rg = Ar, Kr) are characterized by a set of quantum numbers n, l, K and $\mathcal{J}$, where K is the quantum number describing the magnitude of angular momentum $\mathbf{K} = \mathbf{j} + \mathbf{l}$, while $\mathcal{J}$=$K \pm 1/2$ and $j = 3/2, 1/2$ are the total angular momenta of the Rydberg atom and atomic core, respectively. The sublevels $nl[K]_{\mathcal{J}}$ have substantial quantum defects $\delta_{\mathcal{J}}$ at l = 0, 1, 2. On the contrary, for $l \geq$3, the quantum defects are negligible, $\delta_{\mathcal{J}} \approx 0$ [48]. Within the theoretical approach utilized, the effective quantum number was approximated as $n_* = n - \delta_{nl}^{\rm eff}$, where the effective quantum defect $\delta_{nl}^{\rm eff}$ was obtained by averaging over the set of $\delta_{nl[K]_{\rm J}}$ values. The approximation was justified, since $|\delta_{nl}^{\rm eff} - \delta_{nl[K]_{\rm J}}| \ll \delta_{nl}^{\rm eff}$ for l = 0, 1, 2.

The potential energy curves for the electronic states considered, as well as the dipole matrix elements for transitions between terms of $ArXe^+$ and $KrXe^+$ ions, were taken from [24,49]. The ab initio calculations were carried out with the ORCA computer program suite [50] using CASSCF (Complete Active Space Self-Consistent Field) method for 11 electrons in 13 orbitals. The dynamic electron correlation was described in the framework of NEVPT2 theory (n-electron valence state perturbation theory) [51]. Good agreement with existing experimental and theoretical data on the dissociation energies and equilibrium distances of the terms, as well as on the emission spectra of the ions, was demonstrated. The outline of the electronic terms of the ions considered is presented in Figure 2.

The main sources of the uncertainty of the presented theoretical approach are associated with the semiclassical quasicontinuum approximation for rovibrational states, and with the perturbative treatment of the coupling parameter and autoionization width.

The former introduces an error of about 3–6%. For the latter, the estimation of the error depends on specifics of the electronic structure of the molecular cation considered. We believe that for dipole-allowed transitions the overall uncertainty of our method should not exceed 20%.

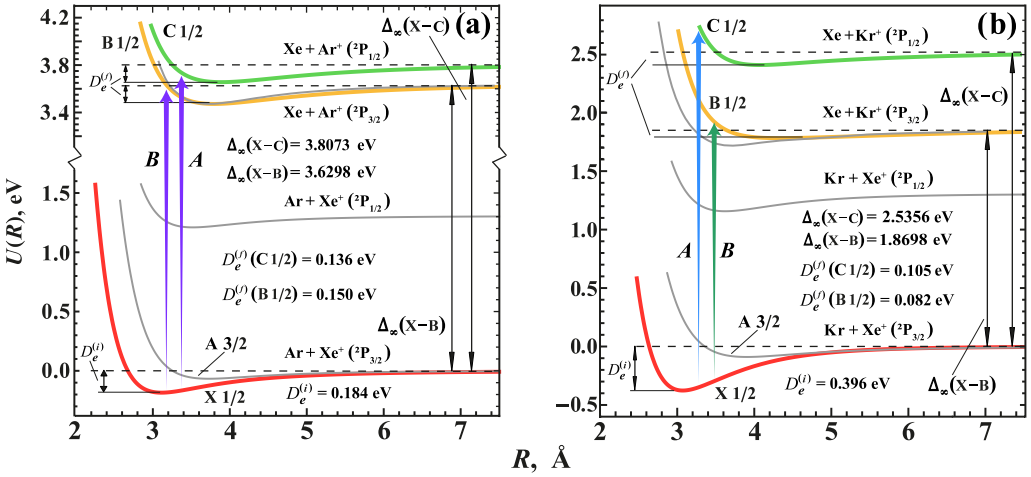

Figure 2. (**a**) Electronic terms of first six electronic states of $ArXe^+$ ion calculated in [24,49]. Values A and B denote the strongest dipole-allowed transitions. (**b**) The same for $KrXe^+$. $\Delta_\infty(X-B)$ and $\Delta_\infty(X-C)$ are the energy separations between the ground state, $X\,1/2$, and excited states with charge transfer characters, $B\,1/2$ and $C\,1/2$, at the dissociation limit ($R \to \infty$).

4. Results

In this section we present the results of calculations of the cross sections of electron-impact dissociative excitation, excitation to a bound state and dissociative recombination processes in collisions involving heteronuclear noble gas ions containing a heavy rare gas element. Specific calculations were carried out for $ArXe^+$ and $KrXe^+$ ions. We show that the efficiency of the aforementioned processes may be quite high when the electronic non-adiabatic transition results in the population of a term with charge transfer character.

4.1. Electron-Impact Dissociative Excitation of Heteronuclear Rare Gas Ions

Below we discuss the dependencies of the Boltzmann-averaged cross sections, $\sigma_T^{\rm de}(\varepsilon)$, of the dissociative excitation (1) of $RgXe^+$ heteronuclear rare gas ions in collisions with electrons on the electron energy, ε, and plasma gas temperature, T. The reaction is realized via non-adiabatic transitions from the ground electronic state resulting in the population of either first excited term, or the terms of charge transfer character (see Section 2). The former were studied in detail previously [22], while the latter, to our knowledge, have not yet been considered theoretically. Similarly to non-adiabatic photoabsorption [24], the transitions to CT states induced by the electron impact are dominated by two most efficient channels of the excitation of the electronic subsystem of the molecular ions: $RgXe^+(X\,1/2) + e \to RgXe^+(C\,1/2) + e \to Xe + Rg^+(^2P_{1/2}) + e$ (type A transitions) and $RgXe^+(X\,1/2) + e \to RgXe^+(B\,1/2) + e \to Xe + Rg^+(^2P_{3/2}) + e$ (type B transitions). Since the energies of the dissociation limits of the ground and CT terms differ substantially, the reaction has a threshold and requires the incident electrons to have kinetic energies of a few eV.

Presented in Figures 3 and 4 are the calculated cross sections, $\sigma_T^{\rm de}(\varepsilon)$, of the dissociative excitation of $ArXe^+$ and $KrXe^+$, respectively, as functions of the energy of the incident electron, ε. Owing to the threshold, the cross sections exhibited a sharp rise at low energies, followed by a distinct maximum, and a slow decrease at high ε. It should be noted that non-adiabatic transfer of large energies of the outer electron to the internuclear motion requires the transitions to occur at $R_{\rm min}(\varepsilon) < R_e^{(i)}$ (see Figure 1 and Equation (8)). The probability of such transitions are exponentially small at $R_0^{(i)} < R_{\rm min}(\varepsilon) < R_e^{(i)}$ and are energetically forbidden at $R_{\rm min}(\varepsilon) < R_0^{(i)}$. Thus, at high ε the reaction is accompanied by small electron

energy loss. Then, the behavior of $\sigma_T^{de}(\varepsilon)$ at $\varepsilon > \Delta U_{fi}(R_0^{(i)})$ is described well by $1/\varepsilon$ dependence, as directly follows from Equation (8).

The position of the maxima for both $ArXe^+$ and $KrXe^+$ shifted to higher energies from $\Delta U_{fi}(R_e^{(i)})$, which, as was shown in [24], corresponds to the maximum of the cross section of the photodissociation. The analysis of the numerical results suggests that, for the cross sections of the dissociative excitation leading to the population of charge transfer terms, the positions of the maxima can be approximated as $\varepsilon_{max} \approx \Delta U_{fi}(R_e^{(i)}) + 0.5$ eV for $ArXe^+$ and $KrXe^+$ ions.

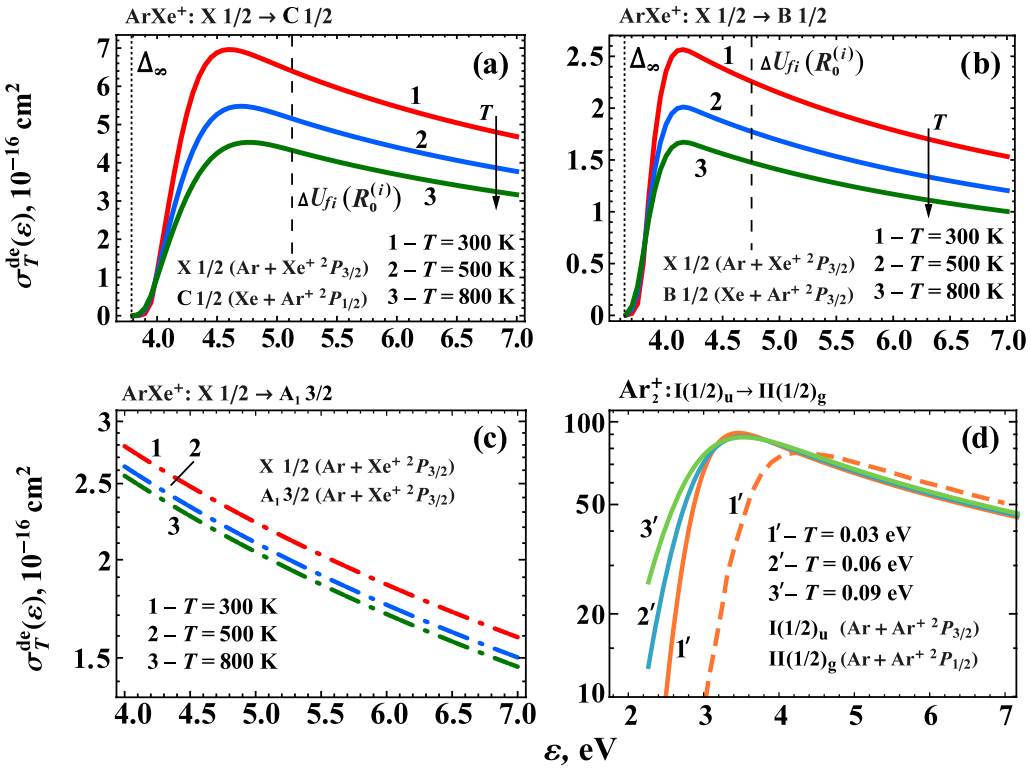

Figure 3. (**a**,**b**) Cross sections of dissociative excitation, σ_T^{de}, of $ArXe^+$ by electrons via transitions to charge transfer terms: $ArXe^+(X\,1/2) + e \rightarrow ArXe^+(C\,1/2) + e \rightarrow Xe + Ar^+(^2P_{1/2}) + e$ ((**a**), A-type transitions) and $ArXe^+(X\,1/2) + e \rightarrow ArXe^+(B\,1/2) + e \rightarrow Xe + Ar^+(^2P_{3/2}) + e$ ((**b**), B-type transitions) at gas temperatures $T = 300$, 500, 800 K. (**c**) Cross sections of dissociative excitation of $ArXe^+$ via non-adiabatic $ArXe^+(X\,1/2) + e \rightarrow ArXe^+(A_1\,3/2) + e \rightarrow Ar + Xe^+(^2P_{3/2}) + e$ transitions at $T = 300$, 500, 800 K. (**d**) Cross sections of process (1) of homonuclear ions Ar_2^+ via $Ar_2^+(I\,1/2_u) + e \rightarrow Ar_2^+(II\,1/2_g) + e \rightarrow Ar + Ar^+(^2P_{1/2}) + e$ transitions at $T = 0.03$, 0.06, and 0.09 eV calculated in [22] (solid lines) and [52] (dashed lines, recalculated in present work).

It is evident from Figures 3a,b and 4a,b that, for both $ArXe^+$ and $KrXe^+$, the transitions of A type, $X\,1/2 \rightarrow C\,1/2$, turned out to be significantly stronger. The respective cross sections of dissociative excitation were 2.5–4 times higher than those corresponding to B type transitions. One can see that, for $ArXe^+$, the profiles of the cross sections in Figure 3a,b were situated in nearly the same electron energy ranges. Thus, Ar^+ ions in the final channel of reaction (1) would mainly populate the $^2P_{1/2}$ state. In contrast, in $KrXe^+$, the maxima of the cross sections corresponding to transitions of A and B types were well separated (by about 0.8 eV), so that, depending on the magnitude of ε, different fine structure components of Kr^+ ($^2P_{1/2}$ or $^2P_{3/2}$) would get populated by electron-impact dissociative excitation.

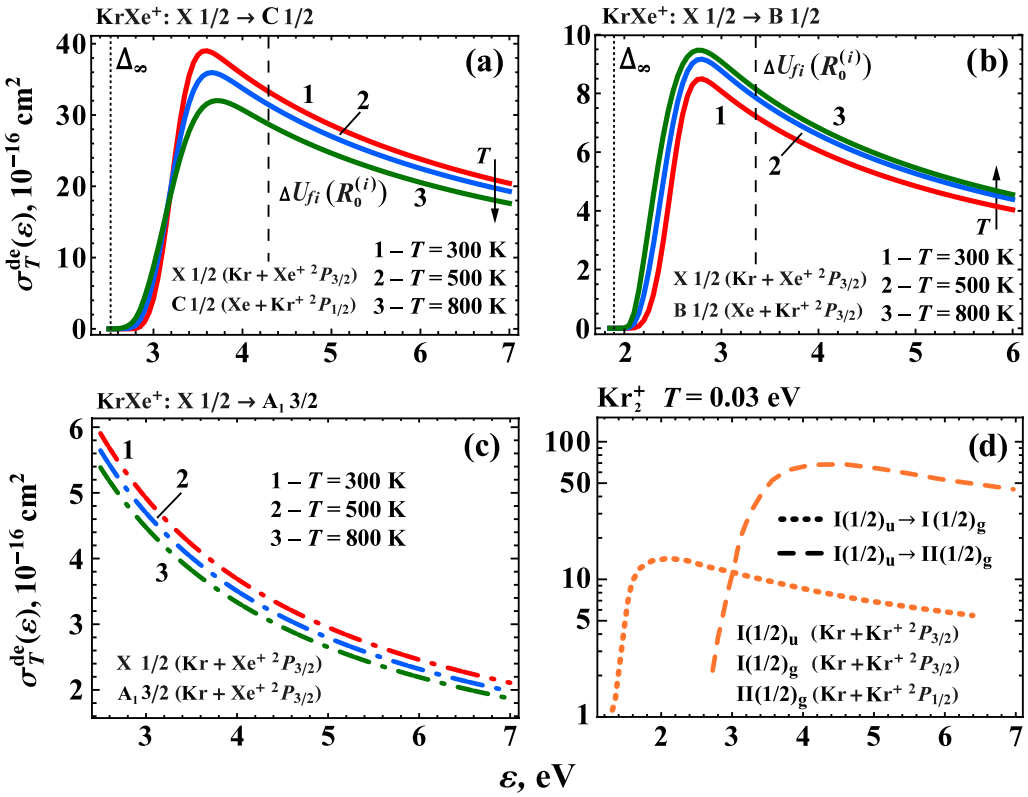

Figure 4. (**a**,**b**) Same as in Figure 3a,b for $KrXe^+$. (**c**) Cross sections of dissociative excitation, $\sigma_T^{\rm de}$, of $KrXe^+$ ions via $KrXe^+(X\,1/2) + e \rightarrow KrXe^+(A_1\,3/2) + e \rightarrow Kr + Xe^+(^2P_{3/2}) + e$ to first excited state $A_1\,3/2$ transitions at $T = 300$, 500, 800 K. (**d**) $\sigma_T^{\rm de}$ for homonuclear ions Kr_2^+ and $Kr_2^+(I\,1/2_u) + e \rightarrow Kr_2^+(I\,1/2_g) + e \rightarrow Kr + Kr^+(^2P_{3/2}) + e$ (dotted lines) and $Kr_2^+(I\,1/2_u) + e \rightarrow Kr_2^+(II\,1/2_g) + e \rightarrow Kr + Kr^+(^2P_{1/2}) + e$ (dashed lines) transitions at gas temperatures $T = 0.03$ eV, initially calculated in [52], recalculated in this work.

The magnitudes of the cross sections, $\sigma_T^{\rm de}(\varepsilon)$, calculated for $ArXe^+$ and $KrXe^+$ differed by a factor of 4–6 in favor of the latter. The rather high ratio was a result of the cumulative effect of two factors. First, the dissociation energy of $KrXe^+$, 398 meV [53], was higher than that of $ArXe^+$, 170 meV [14]. This increased the fraction of the molecular ions in the rovibrational states localized near R_e at thermal equilibrium, which brought the dominating contribution to the cross sections. Second, the oscillator strengths of electronic $X\,1/2 \rightarrow C\,1/2$ and $X\,1/2 \rightarrow B\,1/2$ dipole transitions were somewhat higher [24] in $KrXe^+$, further increasing the ratio.

The data presented in Figures 3a,b and 4a,b were calculated for three values of gas temperatures, $T = 300, 500, 800$ K. It is seen that $\sigma_T^{\rm de}(\varepsilon)$ generally decreased with the increase of T, with the exception of $X\,1/2 \rightarrow B\,1/2$ transitions in $KrXe^+$. The slow increase of the cross sections with the increase of T in Figure 4b stemmed from the specifics of the dependence of $|d_{fi}(R)|^2$ in this system: there was a limited range of $R > R_e^{(i)}$ where the matrix element squared rapidly increased with the increase of R. As the equilibrium population of rovibrational states with substantial probability density at $R > R_e^{(i)}$ was higher for higher temperatures, the Boltzmann-averaged cross sections $\sigma_T^{\rm de}(\varepsilon)$ exhibited the increase with the rise of T.

It is instructive to compare the efficiencies of the dissociative excitation reactions which occur via transitions to charge transfer terms and the first excited $A_1 3/2$ term. The latter are plotted in Figures 3c and 4c for $ArXe^+$ and $KrXe^+$, respectively. One can see that in the range of electron energies considered the contribution from the transitions to CT terms was three times higher in the $ArXe^+ + e$ system. For $KrXe^+$, the dissociative excitation accompanied with charge exchange was an order of magnitude more effective than for the

case of transitions to the first excited electronic term. Thus, this channel of the process (1) plays an important role in the dynamics of plasmas containing heavy heteronuclear rare gas ions.

Plotted in Figures 3d and 4d are the Boltzmann-averaged cross sections of dissociative excitation of homonuclear rare gas ions, Ar_2^+ and Kr_2^+, respectively, calculated in [22,52]. The comparison with Figures 3a,b and 4a,b indicates that $\sigma_T^{\rm de}(\varepsilon)$ were much higher for Ar_2^+ than their counterparts for $ArXe^+$. At the same time, the cross sections obtained for A type of transitions in $KrXe^+ + e$ system were of similar magnitudes with those corresponding to $I(1/2)_u \rightarrow II(1/2)_g$ transitions in Kr_2^+. The same can be said about transitions of B type in $KrXe^+ + e$ and $I(1/2)_u \rightarrow I(1/2)_g$ transitions in Kr_2^+. Therefore, in Ar/Xe plasmas the dissociative excitation via population of CT terms mainly affects the concentrations of $ArXe^+$ ions, whereas in Kr/Xe plasmas the process strongly influences the population of fine structure components of Kr^+ ions in the final channel of the reaction.

4.2. Electron-Impact Excitation of $ArXe^+$ and $KrXe^+$ Ions to Bound Rovibrational States in Charge Transfer Electronic Terms

Considered in this section are the processes of electron-impact excitation (2) of the noble gas cations. The electronic subsystem of the ion is promoted from the ground state to a state with CT character, whereas the nuclei undergo a bound–bound transition. As compared to dissociative excitation (1), discussed in the previous section, the molecular cations remain bound after the collision. The electronic part of the problem is similar to that of process (1), so that for $ArXe^+$ and $KrXe^+$ ions, considered herein, among the possible transitions the strongest ones were $X\,1/2 \rightarrow C\,1/2$ and $X\,1/2 \rightarrow B\,1/2$, denoted by A and B, respectively. In Figure 5a,b we present the results of calculation of the cross sections, $\sigma_T^{\rm cte}(\varepsilon)$, of process (2) for $ArXe^+$ at T =300, 500, 800 K. The cross sections demonstrate pronounced threshold behavior. The increase of $\sigma_T^{\rm cte}(\varepsilon)$ at low energies was sharper than that of $\sigma_T^{\rm de}(\varepsilon)$. The minimal electron energy for process (2) was equal to $\varepsilon_{min} \equiv \min(\Delta U_{fi}(R))$. The position of the maximum could be approximated semiclassically as $\varepsilon_{\rm max} = \Delta U_{fi}(R_0^{(f)})$, with $R_0^{(f)}$ determined from condition $U_f(R_0^{(f)}) = U_f(R \rightarrow \infty)$. Rapid increase of $\sigma_T^{\rm cte}(\varepsilon)$ at $\varepsilon_{\rm min} < \varepsilon < \varepsilon_{\rm max}$ was a result of the combined effect of $R_{\rm min}(\varepsilon)$ approaching the equilibrium distance $R_e^{(i)}$ (thus, increasing the fraction of molecular ions participating in the reaction) and the increase of the oscillator strength $f_{fi}(R)$ with the decrease of R. Further increase of electron energy, $\varepsilon \geq \Delta U_{fi}(R_0^{(f)})$, pushed the area of transitions with the deposition of energy ε into the classically-forbidden range, $R_{\rm min}(\varepsilon) \leq R_0^{(f)}$, so that such transitions provided negligible contributions to the integral cross sections $\sigma_T^{\rm cte}(\varepsilon)$. As a result, the cross sections decreased as $1/\varepsilon$ at $\varepsilon \geq \Delta U_{fi}(R_0^{(f)})$.

The comparison of results of Figures 5a,b and 3a,b suggests that, in accordance with Figure 1, the range of electron energies corresponding to the high efficiency of process (2) shifted to lower ε from that of dissociative excitation (1). The position of the maximum, $\varepsilon_{\rm max}$, of $\sigma_T^{\rm cte}(\varepsilon)$ was roughly 0.5 eV less than the position of the maximum of $\sigma_T^{\rm de}(\varepsilon)$, while the magnitudes of the cross sections at maxima, $\max[\sigma_T^{\rm cte}(\varepsilon)]$, were $\sim$ 6 times lower than $\max[\sigma_T^{\rm de}(\varepsilon)]$ for transitions of type A, and $\sim$ 1.6 times lower for type B transitions. It is instructive to directly compare the relative roles of processes (1) and (2) in the total cross section of the electron-impact excitation of the molecular ions. The respective quantities, $\sigma_T^{\rm cte}(\varepsilon)/(\sigma_T^{\rm cte}(\varepsilon) + \sigma_T^{\rm de}(\varepsilon))$, are plotted in Figure 5 for transitions of type A (panel c) and type B (panel d) in $ArXe^+$. At $\varepsilon < \Delta_\infty \equiv \Delta U_{fi}(R \rightarrow \infty)$ dissociative excitation was impossible, due to energy conservation, so that at $\min(\Delta U_{fi}(R)) \leq \varepsilon \leq \Delta_\infty$ the ratios were equal to 1. With the increase of ε the dominating role of the excitation to bound states in charge transfer electronic terms up to the position of the maximum of $\sigma_T^{\rm cte}(\varepsilon)$ reached at $\varepsilon = \Delta U_{fi}(R_0^{(f)})$. Then, the dissociative excitation channel took over. However, due to similar behavior of $\sigma_T^{\rm de}(\varepsilon)$ and $\sigma_T^{\rm cte}(\varepsilon)$ at high ε (ε^{-1}), the ratio did not fall to zero, but instead approached a positive constant. This indicates that electron-impact induced bound–bound transitions

to states with CT character play a significant role, even at very high electron energies, so that its competition with dissociative excitation in plasmas of Ar/Xe mixtures should be accounted for.

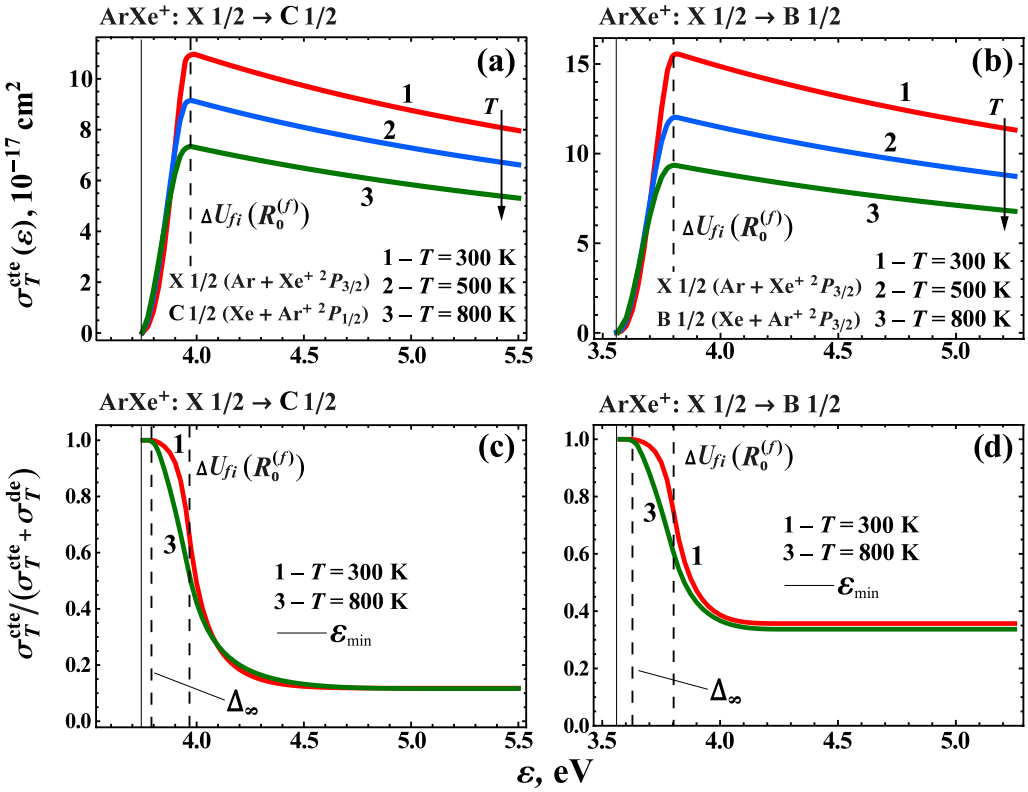

Figure 5. (**a**,**b**) Cross sections of electron-impact excitation σ_T^{cte} of $ArXe^+$ ions to charge transfer states: $ArXe^+(X\,1/2) + e \rightarrow ArXe^+(C\,1/2) + e \rightarrow XeAr^+ + e$ (**a**), A-type transitions) and $ArXe^+(X\,1/2) + e \rightarrow ArXe^+(B\,1/2) + e \rightarrow XeAr^+ + e$ (**b**), B-type transitions) at gas temperatures T = 300, 500, 800 K. (**c**,**d**) Relative contribution, $\sigma_T^{\mathrm{cte}}(\varepsilon)/(\sigma_T^{\mathrm{cte}}(\varepsilon) + \sigma_T^{\mathrm{de}}(\varepsilon))$, of process (2) to the total cross section of charge exchange of $ArXe^+$ ions induced by electron-impact via transitions of type A (**c**) and B (**d**).

It should be noted that such behavior is not universal for all heteronuclear rare gas ions (see below), but stems from the specifics of the initial and final terms of $ArXe^+$. The equilibrium positions for all 3 terms involved in transitions to CT states are quite close. This is also reflected in the nearly absent T-dependence of the ratios. As a result, for any electron energy above threshold the dissociative excitation is accompanied by the formation of bound ions in charge transfer states.

Similar to the data obtained for collisions of $ArXe^+$ with electrons, presented in Figure 5, the results of calculations carried out for the collision system $KrXe^+ + e$ are plotted in Figure 6 for gas temperatures of T =300, 500, 800 K. Overall, the behavior of σ_T^{cte} as a function of ε for $KrXe^+$ ions was like that of $ArXe^+$. As a result of much lower magnitudes of Δ_∞ and $\min(\Delta U_{fi}(R))$, as compared to $ArXe^+$ (see Figure 2), the cross sections exhibited maxima at ε =2.84 and 2.16 eV for transitions of types A and B, respectively. It is evident from Figure 6a,b that, in contrast to $ArXe^+$, the efficiency of process (2) was higher for transitions to $C\,1/2$. The ratio of the magnitudes of the cross sections at the maxima exceeded 6. Nevertheless, since B type transitions may occur at lower electron energies, they cannot be neglected, especially at mean free electron energies below 2 eV.

Relative roles of electron-impact bound–bound excitation (2) and dissociative excitation (1) in the total cross section of electron-impact excitation of $KrXe^+$ to states with charge transfer character, represented by ratios of $\sigma_T^{\mathrm{cte}}(\varepsilon)/(\sigma_T^{\mathrm{cte}}(\varepsilon) + \sigma_T^{\mathrm{de}}(\varepsilon))$, are depicted in Figure 6c,d. One can see that bound–bound transitions brought a significant contribution to the total excitation cross section at relatively short energy range $\varepsilon \lesssim \Delta U_{fi}(R_0^{(f)})$. It

should be noted that, in this range, at T =300 K the absolute values of $\sigma_T^{\rm cte}(\varepsilon)$ were rather low, except for in the vicinity of the maxima. Thus, the role of process (2) in $KrXe^+ + e$ system was not great at room temperatures. At higher ε, the process was suppressed by dissociative excitation. While the ratios approached a constant value, the value was very small, as compared to the case of $ArXe^+$. This was a result of quite different magnitudes of equilibrium distance of lower and upper terms, $R_e^{(f)} \gtrsim R_e^{(i)}$. For bound–bound transition to occur, the molecular ion should be initially localized at quite high internuclear distance $R_{\rm min}(\varepsilon) \approx R_e^{(f)}$. As the depth of the potential well of the ground state of $KrXe^+$ was substantial, the probability of finding the ion at such distances was exponentially small.

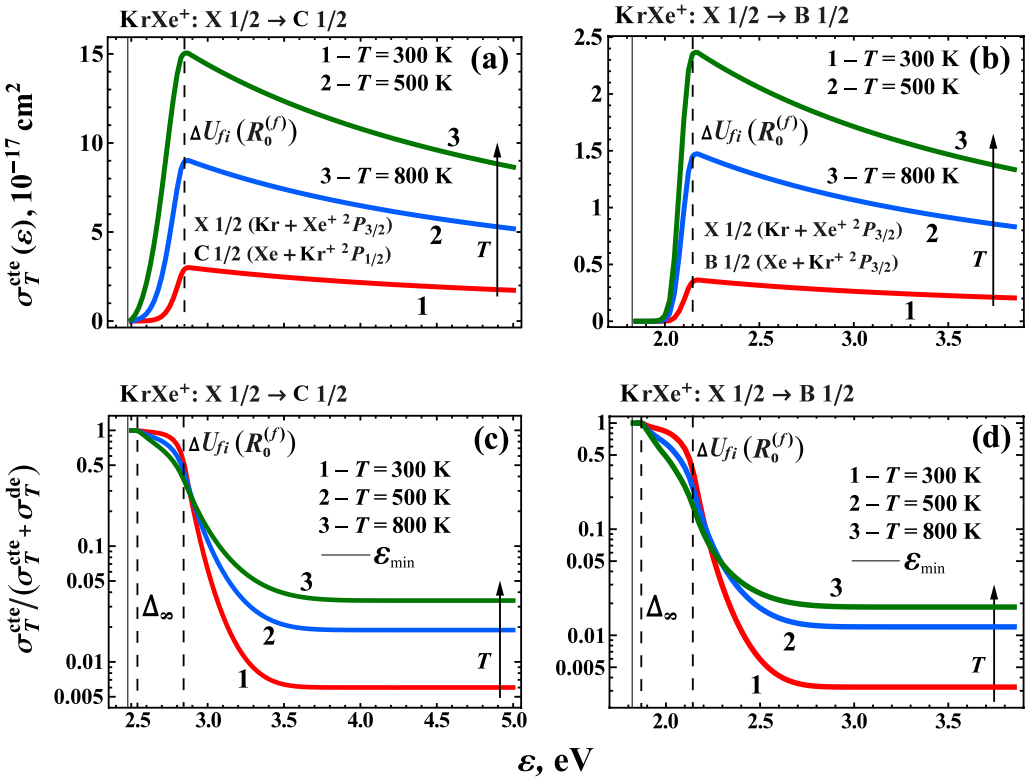

Figure 6. (**a**,**b**) Cross sections of the electron-impact excitation accompanied by charge exchange, $\sigma_T^{\rm cte}$ in $KrXe^+(X\,1/2) + e \rightarrow KrXe^+(C\,1/2) + e \rightarrow XeKr^+ + e$ (**a**) and $KrXe^+(X\,1/2) + e \rightarrow KrXe^+(B\,1/2) + e \rightarrow XeKr^+ + e$ (**b**) collisions at gas temperatures T = 300, 500, 800 K. (**c**,**d**) Relative contribution, $\sigma_T^{\rm cte}(\varepsilon)/(\sigma_T^{\rm cte}(\varepsilon) + \sigma_T^{\rm de}(\varepsilon))$ of process (2) to the total cross section of electron-impact excitation of $KrXe^+$ to CT states via transitions of type A (**c**) and B (**d**).

Quite different positions of lower and upper terms of $KrXe^+$ also manifested in strong dependence of $\sigma_T^{\rm cte}(\varepsilon)/(\sigma_T^{\rm cte}(\varepsilon) + \sigma_T^{\rm de}(\varepsilon))$ on gas temperature T. The increase of T from 300 K to 800 K resulted in a rise of the population of highly-excited rovibrational states, for which the probability density at $R = R_e^{(f)}$ was not negligible. Thus, the magnitude of the ratio increased by a factor of 9. This was also reflected in much stronger T-dependence of $\sigma_T^{\rm cte}$ (see Figure 6a,b). Specifically, the maximal value of $\sigma_T^{\rm cte}$ for transitions of type A increased from 3×10^{-17} cm^2 to 1.5×10^{-16} cm^2, which was comparable with that of $ArXe^+$ ions at T = 800 K. Therefore, at elevated gas temperatures process (2) should be taken into account for both ions considered.

It is instructive to compare the efficiencies of dissociative excitation and electron-impact bound–bound excitation processes, both accompanied by non-adiabatic transitions to charge exchange states. In Figure 7 we show the results of calculations of $\sigma_T^{\rm de}(\varepsilon)$ and $\sigma_T^{\rm cte}(\varepsilon)$ for $ArXe^+$ and $KrXe^+$, summed over the possible transition types. It is seen from the figure that process (1) prevailed in both systems for most electron energies, except for a narrow range of ε near the threshold of dissociative excitation, $\varepsilon = \Delta_\infty$. Nevertheless, as the

products of the reactions under comparison could participate in quite different further processes considered in various kinetic models of lasers and UV sources, it was likely that contributions from dissociative excitation and electron-impact bound–bound excitation would have to be taken in the active level population schemes. It is also worth noting that, in $ArXe^+$, the profiles of the cross sections of both processes, summed over the transition types, were dominated by *A*-type transitions, with those of *B*-type being important in the range of low ε. Thus, it would be difficult to experimentally study the reaction using only an analysis of the scattered electrons. On the contrary, in $KrXe^+$, the overlap of the contributions from both types of transitions strongly distorted the profile of ε-dependence of both dissociative excitation and electron-impact bound–bound excitation, making the assignment of the products easier.

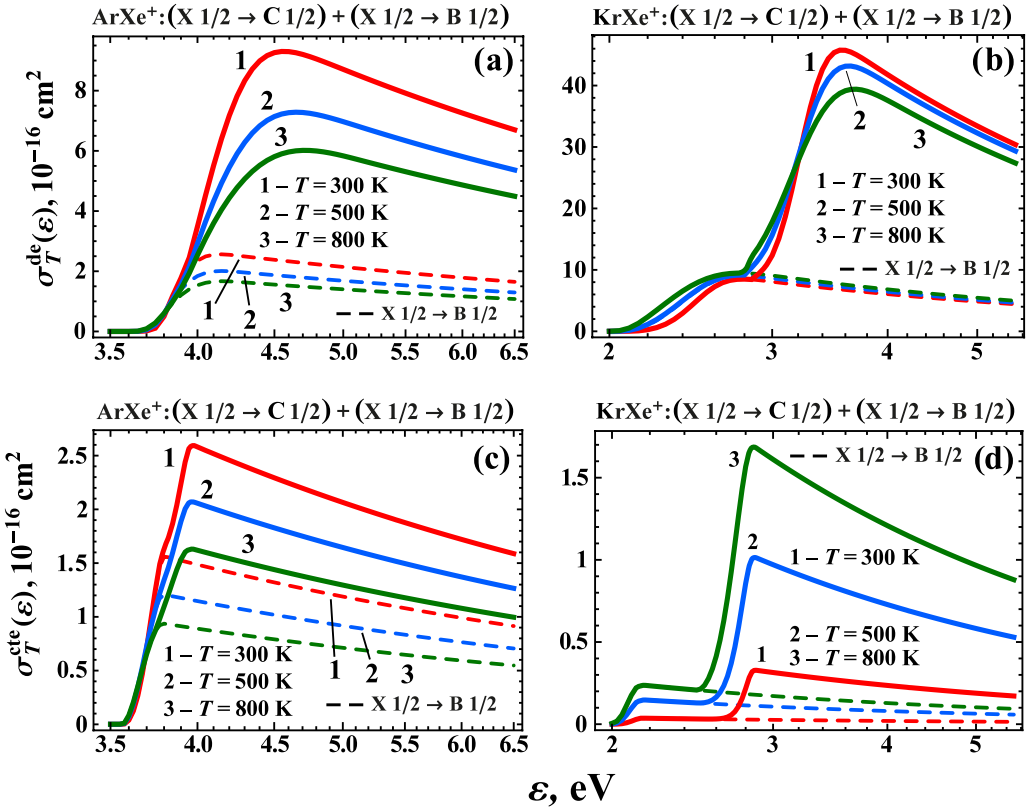

Figure 7. Cross sections of dissociative excitation (1) and electron-impact bound–bound excitation (2) processes accompanied by transitions to charge transfer terms as functions of the incident electron energy for both *A*- and *B*- types of non-adiabatic transitions in $ArXe^+$ and $KrXe^+$ ions at gas temperatures T = 300, 500 and 800 K. (**a**) Cross sections of dissociative excitation in collisions involving $ArXe^+$. (**b**) Cross sections of dissociative excitation in collisions involving $KrXe^+$. (**c**) Cross sections of bound–bound excitation in collisions involving $ArXe^+$. (**d**) Cross sections of bound–bound excitation in collisions involving $KrXe^+$.

4.3. Dissociative Recombination of $RgXe^+$ Ions via Transitions to Charge Transfer States

In contrast to dissociative excitation (1) and bound–bound electron impact excitation (2), considered in Sections 4.1 and 4.2, the incident electron is captured to a bound state in the final channel of the dissociative recombination process (3). In most studies of the direct mechanism of DR of $RgXe^+$ ions with electrons, the reaction was accompanied by the transition of the molecular ion to the first excited term, so that the recombining electron populated one of Xe I levels after the reaction. However, if the kinetic energy of the electron is sufficiently high, the $RgXe^+ + e$ system may undergo a non-adiabatic transition to one of charge transfer terms, which allows the electron to be captured to a Rydberg state of the lighter element, Rg(*nl*). In this section, we discuss the results of

calculations of the cross sections of the process (3) for $ArXe^+$ and $KrXe^+$ ions leading to the population of Ar(n) and Kr(n) Rydberg level, respectively. For strong dipole-allowed transitions, $X\,1/2 \to C\,1/2$ and $X\,1/2 \to B\,1/2$, of $RgXe^+$ molecular ions, the electrons were captured to $Rg(^2P_{1/2}\,n)$ and $Rg(^2P_{3/2}\,n)$ states. Similarly to the previous sections, we denote these types of transitions as A and B, respectively.

Plotted in Figure 8 are the cross sections, $\sigma_n^{\rm dr}(\varepsilon, T)$, of the dissociative recombination (3) of $ArXe^+$ ions accompanied by type A (Figure 8a,c) and B (Figure 8b,d) non-adiabatic transitions, resulting in the electron capture to Ar(n) states, $n = 10, 11, 12$. The cross sections were obtained by the summation over all nl-sublevels with a given value of the principal quantum number n,

$$\sigma_n^{\rm dr}(\varepsilon, T) = \sum_{l=0}^{n-1} \sigma_{nl}^{\rm dr}(\varepsilon, T). \tag{18}$$

To clarify the role of the quantum defects of states with $l \le 3$, panels a and b of Figure 8 depict the results of calculations with the assumption of $\delta_l = 0$, whereas panels c and d show $\sigma_n^{\rm dr}(\varepsilon, T)$ determined with the account for non-zero δ_l.

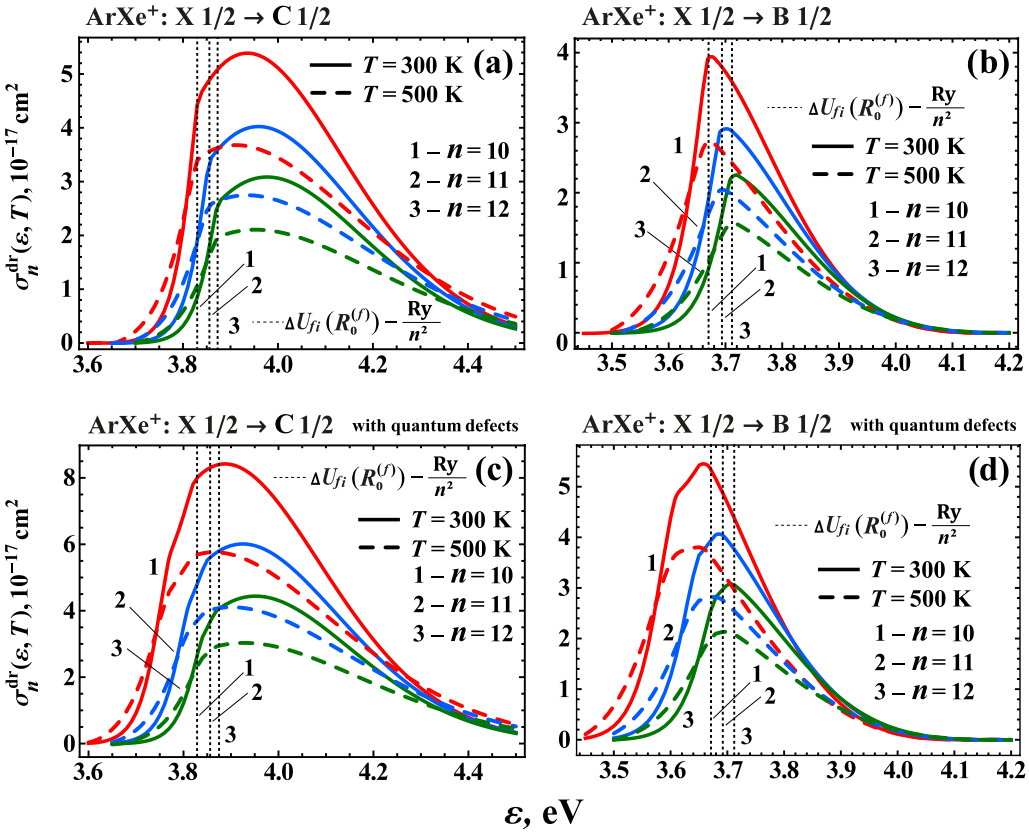

Figure 8. Cross sections of dissociative recombination (18) of $ArXe^+$ ions in collisions leading to population of any nl-sublevels of Ar(n) states with n = 10, 11, 12 calculated without (**a**,**b**) and with (**c**,**d**) the account of non-zero quantum defects of low-l states. (**a**,**c**): reactions accompanied by A-type transitions, $ArXe^+(X\,1/2) + e \to ArXe(C\,1/2, nl) \to Xe + Ar(^2P_{1/2}\,nl)$. (**b**,**d**): same for B-type transitions, $ArXe^+(X\,1/2) + e \to ArXe(B\,1/2, nl) \to Xe + Ar(^2P_{3/2}\,nl)$. Calculations were carried out for gas temperatures T = 300 and 500 K.

The cross sections, $\sigma_n^{\rm dr}(\varepsilon, T)$, are distorted and bell shaped, with distinct maxima. The positions of the maxima can be well approximated by the condition that the process is most efficient when the non-adiabatic transition occurs in the vicinity of the equilibrium distance of the ground state term. If one neglects the quantum defects of states with low l, then the condition can be written as $\varepsilon_{\rm max} \approx \Delta U_{fi}(R_e^{(i)}) - {\rm Ry}/n^2$. Thus, as n increased, the position of the maximum of $\sigma_n^{\rm dr}(\varepsilon, T)$ slowly shifted to the high energy range, which

can be seen in Figure 8. The magnitudes of the cross sections at maxima were several units of 10^{-17} cm^2. Rapid decline of the cross sections with the decrease of ε was caused by the energy conservation law.

Here it is worthwhile to point out that, in this section, we only consider the DR process accompanied by the transitions to charge exchange terms. These states are well-separated energetically (by Δ_∞) from the ground state in the dissociation limit (see Figures 1 and 2). As a result, for the electron capture to Rydberg states of argon with effective principal quantum number $n_* \gg 1$ the energy conservation and the boundary conditions of DR (nuclei should be in a free state after the reaction) set the threshold for the process, $\varepsilon > \Delta_\infty - Ry/n_*^2$. This is in contrast to the standard behavior of $\sigma_n^{\rm dr}(\varepsilon, T)$ which do not vanish at low ε (see, for example, [36,41]). Such a difference is explained by the fact that the dynamics of the dissociative recombination are primarily described as a transition of a $BA^+ + e$ neutral system to a repulsive final state. The electronic state of the ionic core, BA^+, of the neutral system in the final channel of the reaction, can be often approximated by the potential energy curve of first excited electronic state of BA^+, which converges to the same dissociation limit as the ground state of BA^+. For $RgXe^+$ ions, these terms are $|A3/2\rangle$ and $|X1/2\rangle$ (see Figure 2). It is evident that for such a pair of initial and final electronic terms one has $\Delta_\infty = 0$, and the process has no threshold. The dissociative recombination of $RgXe^+$ ions with electrons accompanied by the transitions to $|A3/2\rangle$ state was recently considered in [20,21], and, indeed, the calculated cross sections and rate constants had no threshold. On the contrary, when the final state of the molecular ionic core has charge transfer character, the cross sections, $\sigma_n^{\rm dr}(\varepsilon, T)$, of the dissociative recombination naturally exhibit threshold behavior dependent on the magnitude of the principal quantum number n (see, for example, [25,27]).

When the non-adiabatic transitions occurs at $R_\omega \geq R_0^{(f)}$ (see Figure 1), the energy of the internuclear motion after the electron capture may become negative if the rovibrational energy of the molecular ion in the initial state is not high. Then, the final state is quasi-stationary and decays via various autoionization and dissociation mechanisms [54] not considered in the present work. Respective energy ranges are indicates by the dotted vertical lines in Figure 8 for $n = 10$, 11 and 12.

Comparison of the results plotted in panels (a,b) and (c,d) of Figure 8 clearly demonstrates the significant role of the capture to low-l states characterized by substantial quantum defects δ_l. Due to $\delta_l \neq 0$, the profiles of $\sigma_n^{\rm dr}(\varepsilon, T)$ were formed by the overlap of the profiles corresponding to the individual values of the effective quantum number $n_* = n - \delta_l$, similar to those plotted on panels a and b, but shifted in accordance with the difference between n_* and n. The resulting profiles were appreciably broadened, and the respective maxima positions shifted by $\Delta\varepsilon \sim 0.05$–$0.1$ eV towards smaller energies. It is important to note that the magnitudes of $\sigma_n^{\rm dr}(\varepsilon, T)$ at maxima were $\sim$1.4–1.5 times greater than those obtained in calculations carried out without quantum defects. Thus, correct description of the level structure of Ar(nl) Rydberg states is crucial for a reliable description of the dissociative recombination process, accompanied by transitions to charge transfer terms.

In Figure 9, we present the results of calculations of the cross sections of DR of $KrXe^+$ molecular ions with electrons, resulting in the electron capture to Kr(n) Rydberg states, $n = 10, 11, 12$. Similar to $ArXe^+$, $\sigma_n^{\rm dr}(\varepsilon, T)$ had a distinct maximum. The position of the maximum exhibited weak dependence on the principal quantum number n. As n increased, the maximum slowly shifted to higher ε, and the magnitudes of the cross sections at maximum decreased as $1/n^3$. Unlike the cross sections presented in Figure 8, the profiles of $\sigma_n^{\rm dr}(\varepsilon, T)$ obtained for $KrXe^+$ had the shape of an almost symmetric bell. Such behavior was due to the fact that the potential wells of the upper and lower terms were strongly shifted (see Figure 2) from each other. This suppressed the role of the formation of the quasi-stationary state responsible for low-ε profile distortion in the $ArXe^+ + e$ system. Moreover, the strong shift of the potential wells reduced the role of quantum defects of Kr(nl) states to the increase of the magnitudes of $\sigma_n^{\rm dr}(\varepsilon, T)$ (in 1.5–1.6 times) as the overlapping profiles corresponding to individual $n_{\rm eff}$ were quite similar in both maximum positions and the overall ε-variation.

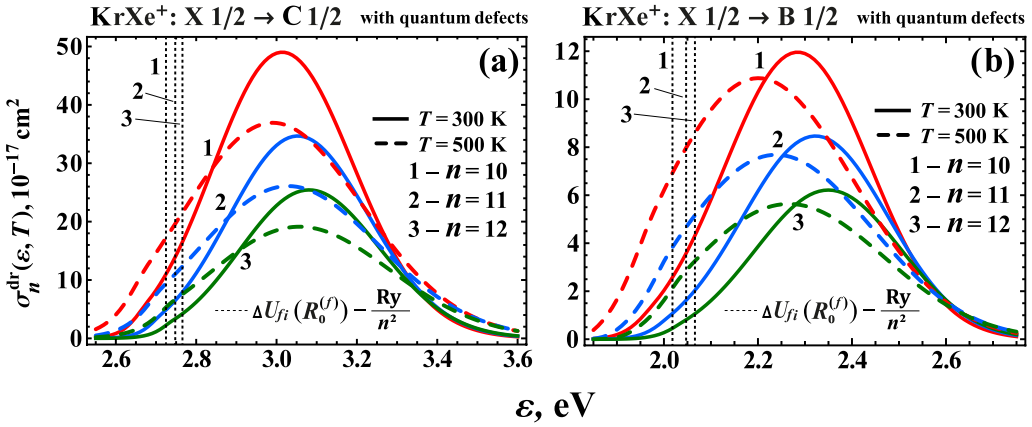

Figure 9. Cross sections of dissociative recombination, $\sigma_n^{\rm dr}(\varepsilon, T)$, of $KrXe^+$ ions followed by population of any nl-sublevel Kr(nl) of Rydberg states with n = 10, 11, 12, realized via non-adiabatic transitions of A-type, $KrXe^+(X\,1/2) + e \to KrXe(C\,1/2, nl) \to\to Xe + Kr(^2P_{1/2}\,nl)$ (**a**) and B-type $KrXe^+(X\,1/2) + e \to KrXe(B\,1/2, nl) \to\to Xe + Kr(^2P_{3/2}\,nl)$ (**b**) at gas temperatures T = 300 and 500 K, calculated with the account for non-zero quantum defects of states with $l \le 3$.

One can also note the unusual T-behavior of $\sigma_n^{\rm dr}(\varepsilon, T)$ calculated for B-type of transitions in $KrXe^+$. As opposed to $ArXe^+$, the maximal values, $\max\left[\sigma_n^{\rm dr}(\varepsilon, T)\right]$, for these transitions only slightly changed as T increased from 300 to 500 K, and the profile of the cross section shifted to smaller ε. Such dependence was mostly a result of the specifics of the dipole transition matrix elements (see also [24]). For $R_\omega \approx R_e^{(i)}$ the magnitude of $|d_{fi}(R_\omega)|^2$ quickly increased with the rise of R. The transitions corresponding to $R_\omega > R_e^{(i)}$ were accompanied by lower electron energy depositions, and the probability of such transition rapidly increased as T is increased.

For both $ArXe^+$ and $KrXe^+$ the values of the cross sections of DR accompanied by the transitions to charge transfer terms were much lower than typical magnitudes of the cross sections of dissociative excitation. However, if one was to compare the roles of the competing dissociation channels (1) and (3), then $\sigma_n^{\rm dr}(\varepsilon, T)$ should be summed over all Rydberg states to which the electron can be captured, $\sigma_{\rm eff}^{\rm dr} = \sum_n \sigma_n^{\rm dr}(\varepsilon, T)$. For $ArXe^+$ and T = 300 K our calculations yielded $\max\left[\sum_{n\ge10} \sigma_n^{\rm dr}(\varepsilon, T)\right] \approx 2.7 \times 10^{-16}$cm^2 for A-type transitions and $\max\left[\sum_{n\ge10} \sigma_n^{\rm dr}(\varepsilon, T)\right] = 2 \times 10^{-16}$cm^2 for B-type transitions. Similarly, for $KrXe^+$ and T = 300 K we obtained $\max\left[\sum_{n\ge10} \sigma_n^{\rm dr}(\varepsilon, T)\right] \approx 2.5 \times 10^{-15}$ cm^2 for A-type transitions, and $\max\left[\sum_{n\ge10} \sigma_n^{\rm dr}(\varepsilon, T)\right] \approx 6 \times 10^{-16}$ cm^2 for transitions of B-type. Therefore, the efficiency of dissociative recombination via charge transfer terms, leading to the population of Rydberg states, is comparable with that of dissociative excitation accompanied by charge exchange.

It should also be noted that the calculated values of $\sigma_n^{\rm dr}(\varepsilon, T)$ were greater than the magnitudes of the cross sections of the dissociative recombination of $ArXe^+$ and $KrXe^+$ accompanied by the transition between the ground and first excited electronic states reported in [21,22], extrapolated to the range of electron energies considered here. This shows that the collisional processes involving transitions to CT states of heteronuclear rare gas cations should be taken into account in cases when the mean plasma electron energies reach several eV.

5. Discussion

Theoretical study of the collisions of electrons with heteronuclear rare gas $RgXe^+$ ions (Rg = Ar, Kr), accompanied by non-adiabatic transitions from the ground state of the molecular ion to electronic terms with charge transfer character, were carried out. Small dissociation energies of the ions resulted in the significant excitation of the quasicontinuum

of the rovibrational states at room and elevated gas temperatures. Three competing reactions were considered: dissociative excitation, electron-impact bound–bound excitation and dissociative recombination. The theoretical treatment of the processes was based on a recently developed approach [20,22,24] and the results [24,49] of ab initio calculations of electronic terms and oscillator strengths of dipole transitions. Significant advantages of the approach used consist in the possibility of self-consistent description of integral contributions from all rovibrational states of $RgXe^+$ and the semi-analytic final expressions for Boltzmann-averaged cross sections of the respective processes. To the authors' knowledge, the reactions considered have not been studied in heavy heteronuclear noble gas cations before.

The cross sections of processes (1)–(3) were calculated at gas temperatures T = 300–800 K. The dependencies of the cross sections on the energy of the incident electron were studied in the range of $\varepsilon = 2$–7 eV, which corresponds to the mean electron energies in typical rare gas excimer lamp [11], powerful Xe I IR lasers [29] and OPRGL [28] setups. We demonstrated that the processes considered were quite effective in this energy range. Due to the presence of two types of charge transfer electronic terms in $RgXe^+$ (Rg = Ar, Kr), the resulting cross sections for each of the processes were formed by the overlap of two bell-shaped profiles, corresponding to the transitions to $C\,1/2$ and $B\,1/2$ states. For collisions involving $ArXe^+$ the overlap produced a single peak with a position dependent on the gas temperature, whereas in $KrXe^+$ the peaks responsible for each of the final terms were clearly distinguishable and did not exhibit T-dependence in the range considered. The magnitudes of the cross sections at the maxima reached several units of 10^{-15} cm^2 for dissociative excitation (1), and several units of 10^{-16} cm^2 for electron-impact bound–bound excitation (2) and dissociative recombination (3) processes. This clearly shows that the reactions discussed herein should be taken into account in kinetic models of the radiation sources above.

It is important to stress that the products of the processes studied, Ar^+, Kr^+, $XeAr^+$, $XeKr^+$, Ar(n), Kr(n), are either commonly used at top levels of the active level population cascades [8,29], or can themselves be the upper levels of active optical transitions. Thus, in addition to complementing the existing kinetic models of powerful UV and IR sources, the results of the present work can serve as a basis for the development of new schemes for the excitation of working radiative transitions.

Author Contributions: Conceptualization, K.K., V.L. and A.N.; methodology, K.K., V.L. and A.N.; validation, K.K., A.N.; formal analysis, K.K. and V.L.; investigation, K.K., V.L. and A.N.; resources, A.N.; writing—original draft preparation, K.K., V.L. and A.N.; writing—review and editing, K.K., V.L. and A.N.; visualization, K.K.; supervision, V.L. and A.N.; project administration, V.L.; funding acquisition, V.L. All authors have read and agreed to the published version of the manuscript.

Funding: This research was funded by the Russian Science Foundation grant number 19-79-30086.

Data Availability Statement: Data supporting the central findings of this study is included in the manuscript.

Conflicts of Interest: The authors declare no conflict of interest. The funders had no role in the design of the study; in the collection, analysis, or interpretation of data; in the writing of the manuscript; or in the decision to publish the results.

Abbreviations

The following abbreviations are used in this manuscript:

VUV	Vacuum ultraviolet
IR	infrared
OPRGL	Optically pumped rare gas lasers
CT	Charge transfer
MQDT	Multi-Channel Quantum Defect Theory
DR	Dissociative recombination
DE	Dissociative excitation

References

1. Cooley, J.E.; Urdahl, R.; Xue, J.; Denning, M.; Tian, P.; Kushner, M.J. Properties of microplasmas excited by microwaves for VUV photon sources. *Plasma Sources Sci. Technol.* **2015**, *24*, 065009. [CrossRef]
2. Park, S.-J.; Herring, C.M.; Mironov, A.E.; Cho, J.H.; Eden, J.G. 25 W of average power at 172 nm in the vacuum ultraviolet from flat, efficient lamps driven by interlaced arrays of microcavity plasmas. *APL Photonics* **2017**, *2*, 041302. [CrossRef]
3. Saidi, S.; Loukil, H.; Khodja, K.; Belasri, A.; Caillier, B.; Guillot, P. Experimental and Theoretical Investigations of Dielectric Barrier Discharge (DBD) Lamp in Ne/Xe Mixture. *IEEE Trans. Plasma. Sci.* **2022**, *50*, 2147–2155. [CrossRef]
4. Kim, H.; Hopwood, J. Scalable microplasma array for argon metastable lasing medium. *J. Appl. Phys.* **2019**, *126*, 163301. [CrossRef]
5. Qu, C.; Tian, P.; Semnani, A.; Kushner, M.J. Properties of arrays of microplasmas: Application to control of electromagnetic waves. *Plasma Sources Sci. Technol.* **2017**, *26*, 105006. [CrossRef]
6. Emmons, D.J.; Weeks, D.E.; Eshel, B.; Perram, G.P. Metastable Ar$(1s_5)$ density dependence on pressure and argon-helium mixture in a high pressure radio frequency dielectric barrier discharge. *J. Appl. Phys.* **2018**, *123*, 043304. [CrossRef]
7. Sun, P.; Zuo, D.; Mikheyev, P.A.; Han, J.; Heaven, M.C. Time-dependent simulations of a CW pumped, pulsed DC discharge Ar metastable laser system. *Opt. Express* **2019**, *27*, 22289. [CrossRef]
8. Kholin, I.V. High-power, high-pressure IR Ar-Xe lasers. *Quantum Electron.* **2003**, *33*, 129. [CrossRef]
9. Han, J.; Heaven, M.C. Gain and lasing of optically pumped metastable rare gas atoms. *Opt. Lett.* **2012**, *37*, 2157–2159. [CrossRef]
10. Gerasimov, G.N. Optical spectra of binary rare-gas mixtures. *Phys.–Usp.* **2004**, *47*, 149–168. [CrossRef]
11. Bhoj, A.N.; Kushner, M.J. Avalanche process in an idealized lamp: II. Modelling of breakdown in Ar/Xe electric discharges. *J. Phys. D Appl. Phys.* **2004**, *37*, 2510–2526. [CrossRef]
12. Emmons, D.J.; Weeks, D.E. Kinetics of high pressure argon-helium pulsed gas discharge. *J. Appl. Phys.* **2017**, *121*, 203301. [CrossRef]
13. Viehl, L.A.; Gray, B.R.; Wright, T.G. Interactions of rare gas cations with lighter rare gas atoms. *Mol. Phys.* **2010**, *108*, 547–555.
14. Zehnder, O.; Merkt, F. The low-lying electronic states of $ArXe^+$ and their potential energy functions. *J. Chem. Phys.* **2008**, *128*, 014306. [CrossRef]
15. Bardsley, J.N.; Biondi, M.A. Dissociative Recombination. In *Advances in Atomic and Molecular Physics*; Bates, D.R., Esterman, I., Eds.; Academic Press: New York, NY, USA; London, UK, 1970; Volume 6, pp. 1–57.
16. Millet, P.; Barrie, A.M.; Birot, A.; Brunet, H.; Dijols, H.; Galy, J.; Salamero, Y. Kinetic study of (ArKr)+ and (ArXe)+ heteronuclear ion emissions. *J. Phys. B At. Mol. Phys.* **1981**, *14*, 459. [CrossRef]
17. Tsuji, M.; Tanaka, M.; Nishimura, Y. New emission spectra of $KrXe^+$ produced from Kr afterglow reactions of Xe. *Chem. Phys. Lett.* **1996**, *262*, 349–354. [CrossRef]
18. Khasenov, M. Emission and level population in noble gases and their binary mixtures under ion beam excitation. *Nucl. Instrum. Methods Phys. Res. B* **2020**, *482*, 45–52. [CrossRef]
19. Samarkhanov, K.; Khasenov, M.; Batyrbekov, E.; Kenzhina, I.; Sapatayev, Y.; Bochkov, V. Emission of Noble Gases Binary Mixtures under Excitation by the Products of the ^{6}Li $(n,\alpha)^3$H Nuclear Reaction. *Sci. Technol. Nucl. Install.* **2020**, *2020*, 8891891.
20. Lebedev, V.S.; Kislov, K.S.; Narits, A.A. Rydberg states population via three-body and dissociative recombination in low-temperature plasmas of rare gas mixtures. *Plasma Sources Sci. Technol.* **2020**, *29*, 025002. [CrossRef]
21. Lebedev, V.S.; Kislov, K.S.; Narits, A.A. Resonant electron capture by ions into Rydberg states of atoms. *J. Exp. Theor. Phys.* **2020**, *130*, 483–498. [CrossRef]
22. Narits, A.A.; Kislov, K.S.; Lebedev, V.S. Semiclassical theory of resonant dissociative excitation of molecular ions by electron impact. *J. Phys. B At. Mol. Opt. Phys.* **2020**, *53*, 195201. [CrossRef]
23. Hausamann, D.; Morgner, H. The heteronuclear rare gas ions: A simple model for the determination of the potential curves. *Mol. Phys.* **1985**, *54*, 1085–1099. [CrossRef]
24. Narits, A.A.; Kislov, K.S.; Lebedev, V.S. Continuous absorption and emission of light by the heteronuclear rare gas $(ArXe)^+$ and $(KrXe)^+$ ions. *J. Chem. Phys.* **2022**, *157*, 204307. [CrossRef]
25. Stroömholmm, C.; Semaniak, J.; Rosén, S.; Danared, H.; Datz, S.; van der Zande, W.; Larsson, M. Dissociative recombination and dissociative excitation of $^4HeH^+$: Absolute cross sections and mechanisms. *Phys. Rev. A* **1996**, *54*, 3086–3094. [CrossRef] [PubMed]
26. Lecointre, J.; Jureta, J.J.; Urbain, X.; Defrance, P. Electron-impact dissociation of HeH^+: Absolute cross sections for the production of He^{q+} (q = 1–2) fragments. *J. Phys. B At. Mol. Opt. Phys.* **2014**, *47*, 015203. [CrossRef]
27. Scarlett, L.H.; Zammit, M.C.; Bray, I.; Schneider, B.I.; Fursa, D.V. Convergent close-coupling calculations of electron scattering on HeH^+. *Phys. Rev A* **2022**, *106*, 042818. [CrossRef]
28. Demyanov, A.V.; Kochetov, I.V.; Mikheyev, P.A.; Azyazov, V.N.; Heaven, M.C. Kinetic analysis of rare gas metastable production and optically pumped Xe lasers. *J. Phys. D Appl. Phys.* **2018**, *51*, 045201. [CrossRef]
29. Ohwa, M.; Moratz, T.J.; Kushner, M.J. Excitation mechanisms of the electron-beam-pumped atomic xenon ($5d \rightarrow 6p$) laser in Ar/Xe mixtures. *J. Appl. Phys.* **1989**, *66*, 5131. [CrossRef]
30. Lebedev, V.S.; Presnyakov, L.P. Photodissociation from a manifold of rovibrational states and free–free absorption by a diatomic molecule. *J. Phys. B At. Mol. Opt. Phys.* **2002**, *35*, 4347. [CrossRef]
31. Jungen, C. *Molecular Applications of Quantum Defect Theory*, 1st ed.; CRC Press: New York, NY, USA, 1996.
32. Tennyson, J. Electron–molecule collision calculations using the R-matrix method. *Phys. Rep.* **2010**, *491*, 29–76. [CrossRef]

33. Khamesian, M.; Ayouz, M.; Singh, J.; Kokoouline, V. Cross Sections and Rate Coefficients for Rotational Excitation of HeH^+ Molecule by Electron Impact. *Atoms* **2018**, *6*, 49. [CrossRef]
34. Mezei, Z.J.; Epée Epée, M.D.; Motapon, O.; Schneider, I.F. Dissociative Recombination of CH^+ Molecular Ion Induced by Very Low Energy Electrons. *Atoms* **2019**, *7*, 82. [CrossRef]
35. Ayouz, M.; Kokoouline, V. Cross Sections and Rate Coefficients for Rovibrational Excitation of HeH^+ Isotopologues by Electron Impact. *Atoms* **2019**, *7*, 67. [CrossRef]
36. Mezei, Z.J.; Chakrabarti, K.; Epée Epée, M.D.; Motapon, O; Yuen, C.H.; Ayouz, M.A.; Douguet, N.; dos, Santos, S.F.; Kokoouline, V.; Schneider, I.F. Electron-Induced Excitation, Recombination, and Dissociation of Molecular Ions Initiating the Formation of Complex Organic Molecules. *ACS Earth Space Chem.* **2019**, *3*, 2376–2389. [CrossRef]
37. Zammit, M.C.; Fursa, D.V.; Savage, J.S.; Bray, I. Electron– and positron–molecule scattering: Development of the molecular convergent close-coupling method. *J. Phys. B At. Mol. Opt. Phys.* **2017**, *50*, 123001. [CrossRef]
38. Rice, O.K. Predissociation and the crossing of molecular potential energy curves. *J. Chem. Phys.* **1933**, *1*, 375. [CrossRef]
39. Lebedev, V.S. Ionization of Rydberg atoms by neutral particles. II. Mechanisms of the perturber-core scattering. *J. Phys. B At. Mol. Opt. Phys.* **1991**, *24*, 1993. [CrossRef]
40. Kislov, K.S.; Narits, A.A.; Lebedev, V.S. Semiclassical Description of Radiative Processes Involving Heteronuclear Molecular and Quasimolecular Rare Gas Ions. *J. Russ. Laser Res.* **2022**, *43*, 556–578. [CrossRef]
41. Larsson, M.; Orel, A.E. *Dissociative Recombination of Molecular Ions*; Cambridge University Press: New York, NY, USA, 2008.
42. Bates, D.R. Super dissociative recombination. *J. Phys. B At. Mol. Opt. Phys.* **1991**, *24*, 703–709. [CrossRef]
43. Pratt, S.T.; Jungen, C. The isotope dependence of dissociative recombination via the indirect mechanism. *J. Chem. Phys.* **2012**, *137*, 174306. [CrossRef]
44. Du, N.Y.; Greene, C.H. Multichannel Rydberg spectra of the rare gas dimers. *J. Chem. Phys.* **1989**, *90*, 6347–6360. [CrossRef]
45. Dehmer, P.M.; Pratt, S.T. Photoionization of ArKr, ArXe, and KrXe and bond dissociation energies of the rare gas dimer ions. *J. Chem. Phys.* **1982**, *77*, 4804–4817. [CrossRef]
46. Sobelman, I.I. *Atomic Spectra and Radiative Transitions*; Springer: Berlin/Heidelberg, Germany, 1979.
47. Lebedev, V.S.; Beigman, I.L. *Physics of Highly Excited Atoms and Ions*; Springer: Berlin/Heidelberg, Germany, 1998.
48. Sukhorukov, V.L.; Petrov, I.D.; Schäfer, M.; Merkt, F.; Ruf, M.-W.; Hotop, H. Photoionization dynamics of excited Ne, Ar, Kr and Xe atoms near threshold. *J. Phys. B At. Mol. Opt. Phys.* **2012**, *45*, 092001. [CrossRef]
49. Narits, A.A.; Kislov, K.S. Electronic Terms and Oscillator Strengths of $ArXe^+$ and $KrXe^+$ Molecular Cations. *Bull. Lebedev Phys. Inst.* **2022**, *49*, 366–372. [CrossRef]
50. Neese, F. Software update: The ORCA program system—Version 5.0. *Wiley Interdiscip. Rev. Comput. Mol. Sci.* **2022**, *12*, e1606. [CrossRef]
51. Angeli, C.; Cimiraglia, R.; Evangelisti, S.; Leininger, T.; Malrieu, J.-P. Introduction of *n*-electron valence states for multireference perturbation theory. *J. Chem. Phys.* **2001**, *114*, 10252. [CrossRef]
52. Marchenko, V.S. Dissociation of homonuclear ions by electron impact. *Sov. Phys. JETP* **1983**, *58*, 292–298.
53. Zehnder, O.; Merkt, F. The low-lying electronic states of $KrXe^+$ and their potential energy functions. *Mol. Phys.* **2008**, *106*, 1215–1226. [CrossRef]
54. Berry, R.S.; Nielsen, S.E. Dynamic Coupling Phenomena in Molecular Excited States. II. Autoionization and Predissociation in H_2, HD, and D_2. *Phys. Rev. A* **1970**, *1*, 395–411. [CrossRef]